Toxicon 215 (2022) 77–90

Contents lists available at ScienceDirect

Toxicon

journal homepage: www.elsevier.com/locate/toxicon

# Developing a computational pharmacokinetic model of systemic snakebite envenomation and antivenom treatment

Natalie M. Morris [*], Johanna A. Blee [**,1], Sabine Hauert [***,1]

*Department of Engineering Mathematics, Ada Lovelace Building, University of Bristol, University Walk, Bristol, BS8 1TW, UK*

ARTICLE INFO

Handling Editor: Ray Norton

*Keywords:*
Snakebite
Antivenom
Venom
Pharmacokinetics
In silico modelling
Computational modelling

ABSTRACT

Snakebite envenomation is responsible for over 100,000 deaths and 400,000 cases of disability annually, most of which are preventable through access to safe and effective antivenoms. Snake venom toxins span a wide molecular weight range, influencing their absorption, distribution, and elimination within the body. In recent years, a range of scaffolds have been applied to antivenom development. These scaffolds similarly span a wide molecular weight range and subsequently display diverse pharmacokinetic behaviours. Computational simulations represent a powerful tool to explore the interplay between these varied antivenom scaffolds and venoms, to assess whether a pharmacokinetically optimal antivenom exists. The purpose of this study was to establish a computational model of systemic snakebite envenomation and treatment, for the quantitative assessment and comparison of conventional and next-generation antivenoms. A two-compartment mathematical model of envenomation and treatment was defined and the system was parameterised using existing data from rabbits. Elimination and biodistribution parameters were regressed against molecular weight to predict the dynamics of IgG, $F(ab')_2$, Fab, scFv, and nanobody antivenoms, spanning a size range of 15–150 kDa. As a case study, intramuscular envenomation by *Naja sumatrana* (equatorial spitting cobra) and its treatment using Fab, $F(ab')_2$, and IgG antivenoms was simulated. Variable venom dose tests were applied to visualise effective antivenom dose levels. Comparisons to existing antivenoms and experimental rescue studies highlight the large dose reductions that could result from recombinant antivenom use. This study represents the first comparative *in silico* model of snakebite envenomation and treatment.

**CREDIT author contributions**

Natalie Morris**: Conceptualization, Methodology, Software, Validation, Formal Analysis, Investigation, Visualization, Writing – Original Draft.**Johanna Blee**: Conceptualization, Methodology, Writing – Review & Editing, Supervision.**Sabine Hauert**: Conceptualization, Methodology, Writing – Review & Editing, Supervision.**

## 1. Introduction

Snakebite envenomation is a neglected tropical disease which globally accounts for over 100,000 deaths and 400,000 cases of disability per year. Snake venom exerts its harmful effects through a complex mixture of protein toxins that target various parts of the body including the blood and the nervous system. The toxin composition of snake venom varies substantially between and within different species (Casewell et al., 2020; Tasoulis and Isbister, 2017). Toxins may act synergistically and may individually vary in toxicity (Laustsen, 2016). There are numerous different toxin families in snake venom, spanning a wide molecular weight range (Tasoulis and Isbister, 2017). Venoms from the elapid family of snakes are typically dominated by low molecular weight toxins, such as three-finger toxins (<10 kDa) and phospholipase $A_2$s (13–15 kDa) (Kini and Doley, 2010; Li et al., 2006; Six and Dennis, 2000). Conversely, viper venoms typically contain more high molecular weight toxins such as snake venom metalloproteinases (20–110 kDa) and snake venom serine proteases (26–67 kDa) (Olaoba et al., 2020; Serrano, 2013; Tasoulis and Isbister, 2017). As molecular size affects the processes of elimination and biodistribution, venoms with different

* Corresponding author.
** Corresponding author.
*** Corresponding author.
*E-mail addresses:* natalie.morris@bristol.ac.uk (N.M. Morris), johanna.benn-blee@bristol.ac.uk (J.A. Blee), sabine.hauert@bristol.ac.uk (S. Hauert).
[1] Authors contributed equally.

https://doi.org/10.1016/j.toxicon.2022.06.006
Received 9 March 2022; Received in revised form 20 May 2022; Accepted 9 June 2022
Available online 15 June 2022

toxin compositions have different pharmacokinetic characteristics. Specifically, smaller toxins generally exhibit faster absorption from the bite site, faster elimination, and greater biodistribution than larger toxins (Gutiérrez et al., 2003). Venoms additionally have variable bioavailabilities. More bioavailable venoms will reach higher concentrations in the blood which may correlate to more severe toxic effects. Less bioavailable venoms may result in increased tissue damage. Owing to this, different venoms may be optimally treated by different antivenom formats. Matching the pharmacokinetic characteristics of antivenoms to their targets has previously been recommended as an approach to improve treatment efficiency, and may have additional benefits in terms of reductions to dosage and side effects (Gutiérrez et al., 2003).

Antivenoms are currently produced by hyper-immunising large mammals such as horses and sheep with sub-lethal doses of venom to stimulate production of toxin-neutralising antibodies. The animals' serum is then harvested and processed to produce the antivenom (León et al., 2018). Conventional serum antivenoms are presently manufactured in three formats: IgGs (150 kDa), and their derivative F(ab')$_2$ fragments (100 kDa) and Fab fragments (50 kDa) (Fig. 1). The smaller fragments have reduced immunogenicity and an increased propensity to perfuse tissue, but also have shorter serum half-lives (Bates and Power, 2019; Gutiérrez et al., 2003; León et al., 2018).

The production and use of serum antivenoms comes with several limitations and drawbacks (Gutiérrez et al., 2017). Since toxin-binding antibodies are rarely purified from the serum, a relatively small proportion of binders in an antivenom may be therapeutically active meaning that large dose volumes are often required. This increases treatment cost and the risk of adverse effects (de Silva et al., 2016). Conventional antivenoms are additionally unable to prevent necrosis due to their poor tissue perfusion and the rapid onset of venom-induced local damage (Gutiérrez et al., 2003). Symptom recurrence may also result from the leaching of toxins from the bite site into the blood over a prolonged period, or from an incomplete initial neutralisation of venom (Boyer et al., 1999; Seifert and Boyer, 2001). There is therefore a strong interest in innovating the design and production of antivenoms.

The recombinant production of antivenoms offers substantial promise in improving the treatment of snakebite. In this method, specific antibodies are produced in heterologous hosts such as bacterial or mammalian cells. As only therapeutically active proteins would be expressed and purified, recombinant antivenoms would have improved safety, efficacy, and potentially cost (Jenkins and Laustsen, 2020; Laustsen et al., 2017). *In vitro* selection methods such as phage display can be used to discover antibodies for recombinant expression. *In vitro* selection averts the requirement of animal immunisation by capturing high affinity binders against specific toxins from large, hypervariable

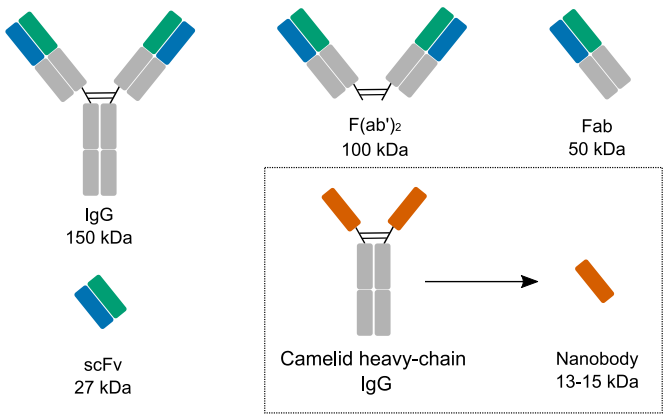


**Fig. 1.** Schematic of the antivenom formats simulated in this study. F(ab')$_2$ and Fab fragments are produced by fragmentation of IgGs. scFvs comprise the linker-connected VL and VH domains from an IgG. Nanobodies are derived from the VHH domain of camelid heavy chain IgGs.

antibody libraries. The use of synthetic antibody libraries can also facilitate the application of alternative scaffolds with novel pharmacokinetic properties (Roncolato et al., 2015; Skerra, 2007). Nanobodies (12–15 kDa) and scFvs (27 kDa) are two alternative antibody fragment scaffolds which are being applied to antivenom development. Nanobodies comprise the VHH binding domain of heavy chain antibodies, which are naturally found in camelids. scFvs comprise the linker-connected variable regions of the light and heavy chain of an IgG (Fig. 1) (Bates and Power, 2019; Hamers-Casterman et al., 1993). Alongside manufacturing and stability benefits, these smaller binders are highly tissue perfusive which may improve their neutralisation coverage (Bates and Power, 2019; Kini et al., 2018; Laustsen et al., 2018b). Recombinant toxin-neutralising antibodies have been successfully produced in a variety of whole IgG and fragmented formats, a summarisation of which has been compiled by Laustsen et al. (2018b).

Pharmacodynamic neutralisation studies have thus far indicated that recombinant antibodies of different formats can neutralise toxins equally well, and there is currently no consensus as to whether there is an ideal antivenom scaffold (Laustsen et al., 2018b). Comparative clinical and pre-clinical studies across the three conventional antivenom formats have variably indicated the importance of scaffold choice on different treatment outcome metrics. Some studies have found scaffold choice to have no significant impact on outcome (Carotenuto et al., 2021; Dart and McNally, 2001; Gerardo et al., 2021; León et al., 2001). Other studies have found there to be significant differences in certain metrics with antivenom choice (Boels et al., 2020; Bush et al., 2015; Ismail and Abd-Elsalam, 1998; León et al., 2001; Mascarenas et al., 2020; Morais et al., 1994; Rivière et al., 1997; Wilson et al., 2022). Given that these studies assess different host species with different venoms and antivenoms, and against different outcome criteria (including survival rate, immunoneutralization, late stage haemotoxicity, and more), the general impact of antivenom scaffold on treatment outcome is unclear. Developing a better understanding of the dynamics of venom-antivenom systems using standardised comparisons across a range of antivenom scaffolds would help ascertain the pharmacokinetic impact of antivenom format on treatment outcome.

To explore the expanding antivenom design space, computational pharmacokinetic simulations could provide a testing ground for the quantitative comparison of both current and next-generation treatments in clinically relevant scenarios. Compartmental models of envenomation and treatment could be used to predict the systemic impact of toxins and the extent of their neutralisation within multiple regions of a virtual body. Such simulations could help elucidate optimal dosing regimes, define antivenom scaffold design rules, and predict the efficacy of novel treatments including combinations of different scaffolds. Computational simulation is faster and cheaper than *in vivo* work, and can enable the systematic assessment of numerous theoretical parameters and treatment scenarios. Computational modelling could also help reduce reliance on animal testing by enabling the *in silico* prototyping of novel treatments. Despite its benefits, pharmacokinetic simulation of envenomation currently represents an underutilised area within the field of snakebite antivenoms. Previously, systemic envenomation by *Tityus discrepans* scorpion venom and its treatment with a F(ab')$_2$ antivenom was compartmentally modelled, however the simulation did not account for the systemic clearance and off-binding effects of the antivenom (Sevcik et al., 2004). More recently, Sanhajariya et al. (2020) simulated mixtures of different toxins non-compartmentally, to explore their variable dispositions and predict overall venom concentrations in the blood.

The aim of this work was to define a computational model of systemic snakebite envenomation and treatment for the comparison of different antivenom scaffolds. In this study, the blood and the tissue were modelled across two compartments, between which venom and antivenom could distribute (Fig. 2). The model was parameterised using experimental pharmacokinetic data from rabbits collected in a literature review, however the equations are completely generalised and could be

used in conjunction with parameters from other model organisms. The distribution and elimination parameters of five antivenom scaffolds (IgG, F(ab')$_2$, Fab, scFv, and nanobody) were predicted based on molecular weight and inputted to the model. As a case study, we apply our model to simulate treatment of systemic *Naja sumatrana* (equatorial spitting cobra) envenomation, a WHO-listed category 1 (highest medical importance) snake found in Southeast Asia, for which there are previously published compartmental pharmacokinetic parameters (Chong et al., 2019; Yap et al., 2014b). Treatment was simulated with Fab, F(ab')$_2$, and IgG antivenoms in different scenarios and compared to existing envenomation treatment studies. Variability to venom dosing was also assessed to explore effective antivenom dose levels. The biological relevance and limitations of our model, its applications to antivenom development, and the dose reduction benefits of recombinant antivenoms are explored in the discussion. This study represents the first comparative pharmacokinetic simulation of envenomation treatment.

## 2. Material and methods

### 2.1. Venom and antivenom compartmental model design

The dynamics of snake envenomation and treatment were described using a two-compartment pharmacokinetic model. Specifically, the elimination and movement of venom, antivenom, and neutralised venom through the blood and the tissue were tracked over time. Data from experimental pharmacokinetic studies of venom and antivenom in rabbits was used to parameterise the model. To establish the known dynamics of venom and antivenom in the body, a literature search was conducted into experimental pharmacokinetic studies of venoms (including isolated venom toxins) and antivenoms on Google Scholar and PubMed. The literature search returned 31 venom and 23 antivenom studies across different species (including mice, rats, rabbits, sheep, humans, cows, and horses). The papers collected are listed in the Electronic Supplementary Materials (ESM, Tables S1, S2). Most of the venom and antivenom studies described a two-compartment pharmacokinetic system with linear elimination, in agreement with a previous review into snake venom pharmacokinetics (Sanhajariya et al., 2018). This structure was consequently chosen to describe the envenomation and treatment model. A compartmental model was utilised to enable tracking of venom and antivenom levels in the tissue, as well as the blood. Compartmental models explicitly separate biodistribution from systemic clearance. This enables quantification of toxins in the tissue (where there may be clinically relevant toxicological effects), and visualisation of the variable dispositions of venoms and antivenoms. This is integral to understanding the extent to which a pharmacokinetic mismatch between venom and antivenom impedes treatment.

The resulting model is shown in Fig. 2, and its parameters are outlined in Table 1. Briefly, the body is divided into a central and a peripheral compartment. The central compartment consists of blood and well-perfused tissues such as the kidneys, liver, and lungs. The peripheral compartment consists of less-well perfused tissues such as muscle and fat (Yates and Arundel, 2008). In the model, venom is intramuscularly absorbed to the central compartment with a limited bioavailability (F). After a time lag, antivenom is intravenously administered to the central compartment as a single bolus dose and can bind and neutralise venom in either compartment. Venom, antivenom, and venom-antivenom complexes can transfer between the two compartments. For simplicity, the elimination of all species in our model was assumed to occur solely in the central compartment. These processes were defined by a series of rate constants. The intramuscular absorption rate is denoted by $k_a$. Transfer from the central to peripheral

**Table 1**
Pharmacokinetic parameters of the two-compartment envenomation and treatment model.

| Parameter | Units | Description |
|---|---|---|
| $k_{10}$ | $h^{-1}$ | Elimination rate constant |
| $k_{12}$ | $h^{-1}$ | Transfer rate constant from central to peripheral compartment |
| $k_{21}$ | $h^{-1}$ | Transfer rate constant from peripheral to central compartment |
| $k_a$ | $h^{-1}$ | Intramuscular absorption rate constant |
| $k_{on}$ | $ml.ng^{-1}h^{-1}$ | Antivenom on-binding rate constant |
| $k_{off}$ | $h^{-1}$ | Antivenom off-binding rate constant |
| $V_c$ | ml | Volume of central compartment |
| $V_p$ | ml | Volume of peripheral compartment |
| F | % | Bioavailability |

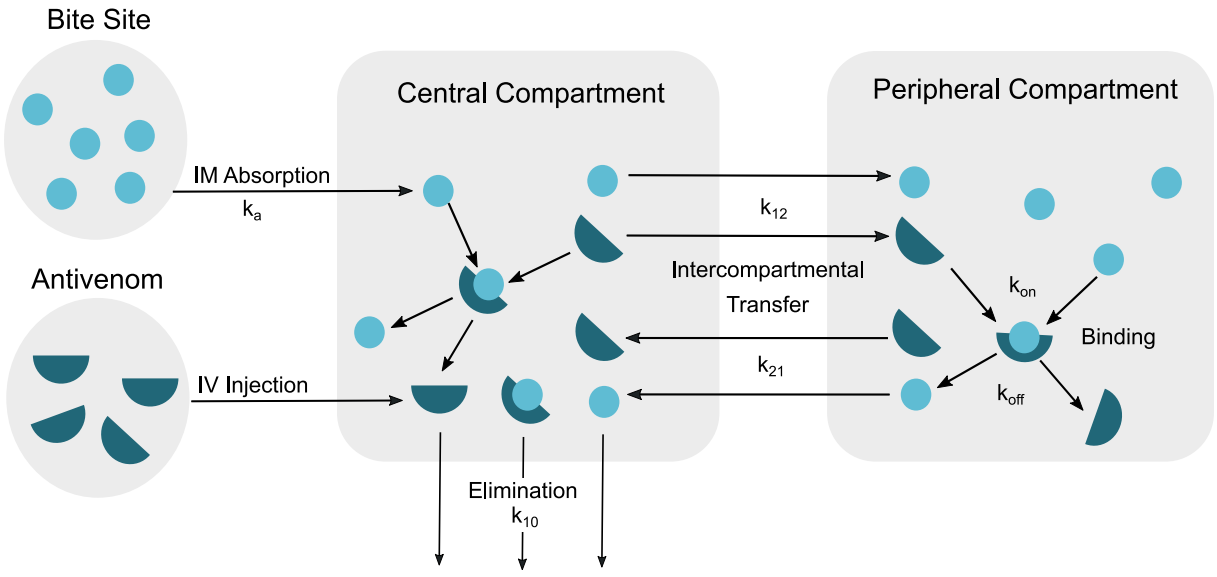


**Fig. 2.** Schematic of the compartmental envenomation and treatment model. Venom toxins are absorbed from the bite site at intramuscular (IM) absorption rate $k_a$. After a delay, antivenom is intravenously (IV) administered to the central compartment. Molecules can diffuse from the central to the peripheral compartment at rate $k_{12}$, and from the peripheral to the central compartment at rate $k_{21}$. Venom can be neutralised in either compartment, with antivenom binding occurring at rate $k_{on}$, and off-binding at rate $k_{off}$. Elimination occurs in the central compartment at rate $k_{10}$. Venom and antivenom have unique $k_{10}$, $k_{12}$, and $k_{21}$ parameter values, and antivenom-venom complexes are assumed to take on the parameter values of the antivenom.

compartment is denoted by $k_{12}$, and transfer back to the central compartment is represented by $k_{21}$. Elimination occurs at rate $k_{10}$. Antivenom binds venom at rate $k_{on}$, and neutralised complexes can spontaneously dissociate at rate $k_{off}$. Neutralised complexes are assumed to take the same dynamics and $k_{10}/k_{12}/k_{21}$ parameter values as the antivenom. The volume of the central compartment is denoted by $V_c$, and the volume of the peripheral compartment by $V_p$. Central and peripheral compartment volumes were assumed to be the same for the venoms and antivenoms, and were assigned using the volumes defined in the venom pharmacokinetic studies. The model was described using systems of ordinary differential equations (ODEs) which were solved numerically in Python.

### 2.2. Intravenous antivenom compartmental model equations

A set of ODE equations was first defined to describe the dynamics of intravenously injected antivenom (Eqs. 1a and 1b). These equations track the change in antivenom mass in each compartment across time. In these equations, A refers to antivenom, 1 to the central compartment, and 2 to the peripheral compartment. Subscript letters signify the species that the parameter is specific to. The intravenously injected antivenom is assumed to have a bioavailability of 100%.

$$\frac{dA1}{dt} = k_{21.A}A2 - (k_{10.A} + k_{12.A})A1 \tag{1a}$$

$$\frac{dA2}{dt} = k_{12.A}A1 - k_{21.A}A2 \tag{1b}$$

### 2.3. Intramuscular envenomation compartmental model equations

Next, intramuscular snake envenomation in the absence of antivenom treatment was defined (Eqs. 2a-d). To facilitate the later use of experimental $k_{on}$ and $k_{off}$ antivenom affinity parameters in the treatment simulations, this equation system was written to follow concentrations. In these equations, the number 1 denotes the intramuscular injection compartment, 2 the central compartment, and 3 the peripheral compartment. T refers to toxins, and E to eliminated toxins. The intramuscular T1 compartment is tracked by mass instead of concentration, as its volume cannot be specified (Eq. 2a).

$$\frac{dT1}{dt} = -k_a T1 \tag{2a}$$

$$\frac{d[T2]}{dt} = \frac{k_a T1 + k_{21.T}[T3]V_p}{V_c} - [T2](k_{10.T} + k_{12.T}) \tag{2b}$$

$$\frac{d[T3]}{dt} = \frac{k_{12.T}[T2]V_c}{V_p} - [T3]k_{21.T} \tag{2c}$$

$$\frac{d[E2]}{dt} = [T2]k_{10.T} \tag{2d}$$

### 2.4. Envenomation and antivenom treatment model equations

To simulate the effect of antivenom treatment on the intramuscular envenomation levels, the venom and antivenom models were combined. Eqs. 2a and 3a-g define the ODE system upon intravenous antivenom administration. The compartments are designated by the same numbering system as the envenomation case, and this equation set additionally introduces neutralised venom-antivenom complexes (N). For the full envenomation and treatment simulations, intramuscular envenomation was first modelled with Eqs. 2a-d for a set time, after which antivenom was introduced and the equation set was switched to Eqs. 2a and 3a-g.

$$\frac{d[T2]}{dt} = \frac{k_a T1 + k_{21.T}[T3]V_p}{V_c} - [T2](k_{10.T} + k_{12.T} + k_{on}[A2]) + k_{off}[N2] \tag{3a}$$

$$\frac{d[T3]}{dt} = \frac{k_{12.T}[T2]V_c}{V_p} - [T3](k_{21.T} + k_{on}[A3]) + k_{off}[N3] \tag{3b}$$

$$\frac{d[A2]}{dt} = \frac{k_{21.A}[A3]V_p}{V_c} - [A2](k_{10.A} + k_{12.A} + k_{on}[T2]) + k_{off}[N2] \tag{3c}$$

$$\frac{d[A3]}{dt} = \frac{k_{12.A}[A2]V_c}{V_p} - [A3](k_{21.A} + k_{on}[T3]) + k_{off}[N3] \tag{3d}$$

$$\frac{d[N2]}{dt} = \frac{k_{21.A}[N3]V_p}{V_c} - \left[N2\right]\left(k_{10.A} + k_{12.A} + k_{off}\right) + k_{on}\left[A2\right]\left[T2\right] \tag{3e}$$

$$\frac{d[N3]}{dt} = \frac{k_{12.A}[N2]V_c}{V_p} - \left[N3\right]\left(k_{21.A} + k_{off}\right) + k_{on}\left[A3\right]\left[T3\right] \tag{3f}$$

$$\frac{d[E2]}{dt} = [T2]k_{10.T} + [N2]k_{10.A} \tag{3g}$$

### 2.5. Envenomation and treatment simulation parameters

The parameter values used in the envenomation and treatment simulations are shown in Table 2. *N. sumatrana* compartmental $k_{10}$, $k_{12}$, $k_{21}$, and F parameters were taken from a previous study (Yap et al., 2014b). $k_a$ was approximated by modelling the venom alone with Eqs. 2a-c, and adjusting $k_a$ to give the originally reported $T_{max}$ (time of maximal blood concentration). The results of this simulation are shown in the ESM (Section 6: Fig. S4; Table S6). In the simulations, intramuscular doses of 0.5 mg/kg or 1.5 mg/kg venom were applied. 0.5 mg/kg has previously been experimentally defined as a sub-lethal intramuscular dose in rabbits (Yap et al., 2014b).

To explore the effect of varying venom dose, we ran the $F(ab')_2$ envenomation-treatment simulations with 0.25, 0.5, and 5 mg/kg venom. The 0.5 mg/kg simulation case was plotted, with the 0.25 and 5 mg/kg cases defining upper and lower bounds for each compartmental concentration curve. In all cases, treatment was simulated with both 2.5 and 7.5 mg/kg antivenom.

### 2.6. Pharmacokinetic parameter compilation

The pharmacokinetic parameters from 1 venom and 11 antivenom

**Table 2**
Envenomation and treatment simulation input parameters.

| Parameter | Value | Unit | Source |
|---|---|---|---|
| $k_{10.Venom}$ | 0.0948 | $h^{-1}$ | Yap et al. (2014b) |
| $k_{12.Venom}$ | 0.4 | $h^{-1}$ | Yap et al. (2014b) |
| $k_{21.Venom}$ | 0.5 | $h^{-1}$ | Yap et al. (2014b) |
| $k_{a.Venom}$ | 2.2 | $h^{-1}$ | Estimated |
| $F_{Venom}$ | 41.9 | % | Yap et al. (2014b) |
| $F_{Antivenom}$ | 100 | % | Assumed |
| $V_c$ | 500 | $ml.kg^{-1}$ | Yap et al. (2014b) |
| $V_p$ | 400 | $ml.kg^{-1}$ | Yap et al. (2014b) |
| $k_{10.IgG}$ | 0.0120 | $h^{-1}$ | Regression prediction |
| $k_{12.IgG}$ | 0.0426 | $h^{-1}$ | Regression prediction |
| $k_{21.IgG}$ | 0.0989 | $h^{-1}$ | Regression prediction |
| $k_{10.Fab2}$ | 0.0212 | $h^{-1}$ | Regression prediction |
| $k_{12.Fab2}$ | 0.0613 | $h^{-1}$ | Regression prediction |
| $k_{21.Fab2}$ | 0.154 | $h^{-1}$ | Regression prediction |
| $k_{10.Fab}$ | 0.0341 | $h^{-1}$ | Regression prediction |
| $k_{12.Fab}$ | 0.114 | $h^{-1}$ | Regression prediction |
| $k_{21.Fab}$ | 0.240 | $h^{-1}$ | Regression prediction |
| $k_{on}$ | $6 \times 10^5$ | $M^{-1}s^{-1}$ | Assumed |
| $k_{off}$ | $1 \times 10^{-3}$ | $s^{-1}$ | Assumed |
| Rabbit weight | 2 | Kg | Assumed |

studies in rabbits were compiled from the literature review and used to parameterise the model (Tables 3–4). The rabbit system was chosen for parameterisation because it was the most frequently used across both venom and antivenom studies. The benefits of the rabbit system are threefold: firstly, the model could potentially be validated in real life. Secondly, rabbits are sufficiently large to enable repeated blood sampling over timecourses relevant to envenoming. Thirdly, the pharmacokinetic parameters of real toxins and venoms can be tested and applied. In these experimental animal tests the entire pharmacokinetic profile of the venom can be recorded and analysed, which enables the detection of early tissue distribution effects which may not be captured in human clinical studies (Sanhajariya et al., 2018).

We aimed to gather as many experimental parameters and metrics from these studies as possible to aid our overall understanding of the system. The antivenom studies collected displayed a large range in elimination half-life. IgGs had a range of 43–2272 h (1.8–95 days), F (ab')$_2$s of 20.3–113 h, and Fabs of 8–89.3 h. In humans, Fab fragments are known to have serum half-lives of 12–20 h and IgGs of 10–21 days (Flanagan and Jones, 2004; Mankarious et al., 1988). Larger animals have slower metabolic rates, leading to slower systemic clearance (Boxenbaum, 1982). Subsequently one would generally expect the antivenom half-lives to be shorter in rabbits than in humans. The reasons for this disparity in the antivenom datasets are unclear, however it is possible that this is a natural deviation since most of the independent Fab antivenom studies showed similarly long elimination half-lives.

Several studies reported $k_{10}$, $k_{12}$, and $k_{21}$ rates and thus could be directly used in our modelling, however most of the papers only reported non-compartmental parameters such as systemic clearance (CL). Where possible, these were transformed into their compartmental counterparts. Eqs. 4a and 4b are standard calculations to transform CL into the elimination rate (Johanson, 2010; Rowland and Tozer, 1995). Eq. 4a was used to estimate antivenom $k_{10}$ since all antivenom studies collected reported volumes of distribution ($V_d$ - specifically, the volume of distribution at steady state, $V_{ss}$). Venom and toxin elimination rates were calculated using Eq. 4b, since these papers quoted the $V_c$ values and defined elimination as occurring predominantly from the central compartment (Yap et al., 2013; 2014b). To verify these rates, the elimination half-lives ($t_{½\beta}$) of the resulting venom and toxin parameter sets were calculated using Eqs. 5a and 5b and compared to the reported values (ESM, Table S3). In these equations, β is the pharmacokinetic constant of the terminal phase.

$$k_{10} = \frac{CL}{V_d} \tag{4a}$$

$$k_{10} = \frac{CL}{V_c} \tag{4b}$$

$$\beta = \frac{1}{2}\left(k_{10} + k_{12} + k_{21} - \sqrt{(k_{10} + k_{12} + k_{21})^2 - 4k_{10}k_{21}}\right) \tag{5a}$$

$$t_2^1\beta = \frac{\ln(2)}{\beta} \tag{5b}$$

Whilst a two-compartment structure was used for the final model, some parameters from three-compartment studies were included in the parameterisation. CL values from two three-compartment studies were transformed into $k_{10}$ rates as this relationship is independent of compartmental structure. Due to a lack of $k_{12}$ and $k_{21}$ parameters in antivenoms, the transfer parameters from two three-compartment models were adapted to our system (Ismail et al., 1998; Ismail and Abd-Elsalam, 1998). In these studies, the three compartments comprise a central compartment of blood, which links separately to a shallow tissue compartment of well-perfused tissue (via $k_{12}$ and $k_{21}$ parameters) and a deep tissue compartment of poorly-perfused tissue (via $k_{13}$ and $k_{31}$ parameters) (Ismail et al., 1996). Since our model assumes that the central compartment consists of both blood and well-perfused tissue, the shallow compartment was assumed to be encompassed within the central compartment of our model, and thus the $k_{13}$ and $k_{31}$ parameters of the deep tissue were taken to represent $k_{12}$ and $k_{21}$. The volumes of the central and shallow tissue compartment in these studies were additionally combined to produce a lumped $V_c$.

**Table 3**
Pharmacokinetic parameters from antivenom studies in rabbits. All studies involve equine derived immunoglobulins and their fragments, and were taken from single bolus IV administrations in non-envenomed rabbits. * Indicates that the $k_{10}$ rate was calculated using $CL/V_{ss}$. Outliers which were excluded from further analyses are shown in italics. Compartment volumes and clearance have been standardised by body weight (BW), using the midpoint of reported rabbit weight ranges. n = sample size. ELISA = Enzyme Linked Immunoabsorbent Assay; RIA = Radioimmunoassay; IRMA = Immuoradiometric Assay.

| Scaffold | $k_{10}$ ($h^{-1}$) | $k_{12}$ ($h^{-1}$) | $k_{21}$ ($h^{-1}$) | T ½ β (h) | CL/BW (ml $h^{-1}$ $kg^{-1}$) | $V_c$/BW (ml $kg^{-1}$) | $V_p$/BW (ml $kg^{-1}$) | $V_{ss}$/BW (ml $kg^{-1}$) | Method | n | Reference |
|---|---|---|---|---|---|---|---|---|---|---|---|
| IgG | 0.00875* | | | 82.3 | 1.97 | 72.7 | | 225 | ELISA | 4 | Quesada et al. (2006) |
| | 0.0148* | | | | 0.74 | | | 50 | ELISA | 4 | Vázquez et al. (2013) |
| | 0.00916 | | | | | | | 95.3 | ELISA | 3 | Navarro et al. (2016) |
| | *0.0003* | | | 2272 | 0.0123 | | | 33 | ELISA | 4 | Herrera et al. (2017) |
| | 0.0139 | | | 50 | 5 | | | 410 | ELISA | 4 | Rojas et al. (2013) |
| | 0.0282 | 0.018 | 0.096 | 42.7 | | 118 | 44 | 162 | RIA | 6 | Ismail et al. (1998) |
| | 0.0240 | 0.042 | 0.102 | 46.5 | | 15 | 6 | 91 | RIA | | Ismail and Abd-Elsalam (1998) |
| | 0.00321* | | | 96.1 | 0.25 | 34 | | 78 | ELISA | 4 | Vázquez et al. (2010) |
| F (ab')$_2$ | 0.0159* | | | | 2.70 | | | 170 | ELISA | 4 | Vázquez et al. (2013) |
| | 0.0124* | | | 61.4 | 1.17 | 46.3 | | 94.1 | RIA | 5 | Bazin-Redureau et al. (1998) |
| | 0.0162* | | | 55 | 2.10 | | | 130 | ELISA | 3 | Rivière et al. (1997) |
| | 0.0528 | 0.204 | 0.21 | 33.8 | | 136 | 82 | 216 | RIA | 6 | Ismail et al. (1998) |
| | 0.066 | 0.504 | 0.426 | 28.3 | | 60 | 52 | 400 | RIA | | Ismail and Abd-Elsalam (1998) |
| | 0.0155* | | | 49.5 | 3.56 | | | 230 | IRMA | 5 | Pépin-Covatta et al. (1996) |
| | 0.007* | | | 113 | 3.88 | 56 | | 554 | ELISA | 4 | Vázquez et al. (2010) |
| | 0.0376* | | | 20.3 | 3.07 | | | 81.6 | ELISA | 4 | El Hafny et al. (2002) |
| Fab | 0.0182* | | | | 4.73 | | | 260 | ELISA | 4 | Vázquez et al. (2013) |
| | 0.230* | | | 8 | 53 | | | 230 | ELISA | 3 | Rivière et al. (1997) |
| | 0.0192 | 0.024 | 0.036 | 54.8 | | 60.8 | 40 | 117 | RIA | 6 | Ismail et al. (1998) |
| | 0.0264 | 0.018 | 0.09 | 62.3 | | 70 | 16 | 300 | RIA | | Ismail and Abd-Elsalam (1998) |
| | 0.0169* | | | 89.3 | 13.61 | 30 | | 807 | ELISA | 4 | Vázquez et al. (2010) |

**Table 4**
Compartmental pharmacokinetic parameters for venoms and toxins in rabbits. * Indicates that the $k_{10}$ rate was calculated using $CL/V_C$. Compartment volumes and clearance have been standardised by body weight (BW), using the midpoint of reported rabbit weight ranges. Accession numbers of toxins are given in brackets where available. n = sample size.

| Species | Venom or Toxin? | Molecular weight (kDa) | Route | $k_{10}$ ($h^{-1}$) | $k_{12}$ ($h^{-1}$) | $k_{21}$ ($h^{-1}$) | F (%) | $T_{max}$ (h) | $k_a$ ($h^{-1}$) | T ½ β (h) | $V_c$ (ml $kg^{-1}$) | $V_p$ (ml $kg^{-1}$) | CL (ml $h^{-1}$ $kg^{-1}$) | n | Method | Reference |
|---|---|---|---|---|---|---|---|---|---|---|---|---|---|---|---|---|
| *Naja sumatrana* | Whole venom | NA | IV | 0.0913* | 0.4 | 0.5 | 100 | | | 13.6 | 500 | 400 | 45.65 | 3 | ELISA | Yap et al. (2014b) |
| | | | IM | 0.0948* | | | 41.9 | 1 | 2.2 | 12.5 | | | 47.4 | 3 | | |
| | $PLA_2$ (Q92084) | 16 | IV | 0.192* | 0.6 | 0.3 | 100 | | | 11.7 | 250 | 450 | 47.9 | 3 | | |
| | | | IM | 0.192* | | | 68.6 | 2 | 0.5 | 10.18 | | | 47.9 | 3 | | |
| | Neurotoxin (Q9PSN6) | 6.5 | IV | 0.182* | 0.7 | 0.6 | 100 | | | 8.8 | 450 | 500 | 82.05 | 3 | | |
| | | | IM | 0.182* | | | 81.5 | 0.5 | 3.8 | 8.9 | | | 82.05 | 3 | | |
| | Cardiotoxin (P60302) | 8 | IV | 0.174* | 0.6 | 0.6 | 100 | | | 8.6 | 500 | 550 | 86.85 | 3 | | |
| | | | IM | 0.174* | | | 45.6 | 0.5 | 3.9 | 8.2 | | | 86.85 | 3 | | |
| | Cardiotoxin (P60302) in venom | 8 | IV | 0.150* | 0.8 | 0.6 | 100 | | | 11 | 400 | 500 | 59.9 | 3 | | |
| | | | IM | 0.152* | | | 39.5 | 0.5 | 3.8 | 11.6 | | | 60.85 | 3 | | |
| *Naja sputatrix* | Whole venom | NA | IV | 0.0859* | 0.9 | 0.9 | 100 | | | 15.4 | 400 | 400 | 34.35 | 3 | ELISA | Yap et al. (2013) |
| | | | IM | 0.0849* | | | 41.7 | 0.75 | 2.6 | 18.9 | | | 33.95 | 3 | | |
| *Cryptelytrops purpureomaculatus* | Whole venom | NA | IV | 0.140 | 2.19 | 0.48 | 100 | | | 27.7 | 390 | 1800 | 54.7 | 3 | ELISA | Sim et al. (2013) |
| | | | IM | 0.141 | | | 41.6 | 1 | 0.7 | 27 | | | 54.8 | 3 | | |

### 2.7. Antivenom and venom parameter regressions

We next sought to define relationships between the $k_{10}$, $k_{12}$ and $k_{21}$ parameters and molecular weight to enable to simulation of scaffolds of variable sizes. We aimed to calculate average $k_{10}$, $k_{12}$, and $k_{21}$ parameters for different antivenom scaffolds, as there was significant variability in the reported pharmacokinetic metrics (i.e. elimination half-life) and profiles (ESM, Section 5: Figs. S2-S3) of the same scaffold type across different studies. Parameters from 1 venom and 11 antivenom studies were regressed against molecular weight, with the inputted parameters outlined across Tables 3–4 Low molecular weight toxins were included to enable simulation of small scaffolds such as nanobodies and scFvs in the absence of experimental data for these fragments. The regression models were selected based on the underlying biology of each relationship, which is explained further in the ESM (Section 3). The $k_{10}$ data was regressed against Eq. 6, a modified sigmoid originally defined by Li et al. (2017) to relate molecular size to CL. IgGs were not included in this regression since they are recycled through the FcRn system which extends their half-life (Ober et al., 2004). The IgG $k_{10}$ value was instead estimated by taking the geometric mean of these datapoints. One IgG $k_{10}$ was marked as an outlier: the explanation of this and the resulting IgG dynamics inclusive of this datapoint are detailed in the ESM (Section 4: Fig. S1; Table S4).

$$ln(k_{10}) = 1 - \frac{c}{1 + \exp(b(-MW + a))} \tag{6}$$

The $k_{12}$ data was regressed against a logarithmic model (Eq. 7), the shape of which reflects the variable transfer of differently sized molecules across the two pore types found in capillaries (Li and Shah, 2019). The $k_{21}$ data was regressed against a linear model (Eq. 8), to reflect the previously described relationship between molecular size and lymphatic uptake (Wu et al., 2012). In Eqs. 6–8, MW denotes molecular weight and is given in kDa.

$$ln(k_{12}) = a\ln(MW) + b \tag{7}$$

$$ln(k_{21}) = aMW + b \tag{8}$$

### 2.8. Simulating the predicted antivenom parameter sets

To analyse the dynamics arising from the regressions, simulations of nanobody, scFv, Fab, $F(ab')_2$, and IgG antivenoms were conducted using the parameter predictions at 15, 27, 50, 100, and 150 kDa, respectively. The antivenoms were modelled using Eqs. 1a and 1b, with a starting mass of 1000 ng. The elimination half-lives of the antivenoms were calculated using Eqs. 5a and 5b. The biodistribution constant (BD) defined by Shah and Betts (2013), was adapted and applied in Eq. 9. Whilst the standard BD equation utilises concentrations in the blood and specific organs, here the BD was calculated using raw compartmental masses sampled from an elimination phase timepoint.

$$BD\ (\%) = \frac{Peripheral\ Mass}{Central\ Mass} \times 100 \tag{9}$$

### 2.9. Software

All regression and ODE simulations were coded in Python using JupyterLab 1.2.6. Specific packages used were NumPy 1.18.1, matplotlib 3.1.3, and Scipy 1.4.1. Python scripts are available at https://bitbucket.org/hauertlab/venom-antivenom-model/src/main/. Figs. 1 and 2 were produced in Inkscape. All other figures were produced in Python using matplotlib.

## 3. Results

### 3.1. A mathematical model of systemic snakebite envenomation and treatment

We defined a mathematical model of systemic snake envenomation and antivenom treatment, using a two-compartment pharmacokinetic system with linear elimination from the central compartment (Fig. 2). In this model, the body is divided into a central compartment of well-perfused tissues and a peripheral compartment of less-well perfused tissues. Venom is introduced to the central compartment at a set intramuscular absorption rate, and after a time delay antivenom is intravenously administered as a single bolus dose. Once inside the compartmental system, both venom and antivenom can move between the compartments at given rates. Antivenom can bind venom in either compartment, and neutralised complexes can spontaneously dissociate. Neutralised complexes are assumed to take the same pharmacokinetic parameters as the antivenom. The model can track the levels of venom, antivenom, neutralised venom, and eliminated venom in each compartment across time. Whilst simulations were based on rabbit pharmacokinetic data, parameters from other species could be applied to the model.

### 3.2. Molecular weight can be used to predict antivenom elimination and biodistribution parameters

To obtain averaged pharmacokinetic parameters for antivenom scaffolds of different sizes, we conducted a series of linear and nonlinear regressions on venom and antivenom $k_{10}$, $k_{12}$, and $k_{21}$ rates collected in a literature review. The resulting regression coefficients and their standard errors are recorded in Table 5, and the regression plots are shown in Fig. 3. The relationship between these parameters and molecular weight can be used to assess the impact of antivenom scaffold size on venom neutralisation.

The $k_{10}$ elimination parameter was regressed against a sigmoidal model (Fig. 3a). The $k_{10}$ regression had a generally good prediction efficacy, with 71% of datapoints lying within the two-fold error envelope. A logarithmic model was chosen to fit the $k_{12}$ data (Fig. 3b). Due to the sparse and noisy underlying data, the $k_{12}$ regression line has a poorest prediction capacity with 50% of datapoints lying within the two-fold error envelope. A linear model was used to fit the $k_{21}$ data (Fig. 3c), with 70% of datapoints laying within the two-fold error envelope. In the $k_{12}$ and $k_{21}$ regressions, the data for the 50 kDa Fabs cluster with slower rates than the $F(ab')_2$ and IgG antivenoms. This is indicative of poorer tissue perfusion which contradicts the expected behaviour. This poorer Fab tissue perfusion was explicitly noted in the original papers also, and thus does not seem to be a result of collapsing the original three-compartment model (Ismail et al., 1998; Ismail and Abd-Elsalam, 1998).

### 3.3. Compartmental modelling using predicted antivenom parameters replicates the anticipated elimination and biodistribution behaviours

The regression models were used to predict the compartmental parameters of intravenously injected IgGs, $F(ab')_2$s, Fabs, scFvs, and nanobodies (Table 6). These predictions were used to simulate the compartmental dynamics of each antivenom (Fig. 4). We also calculated the elimination half-lives and the biodistribution ratios of each antivenom (Table 6).

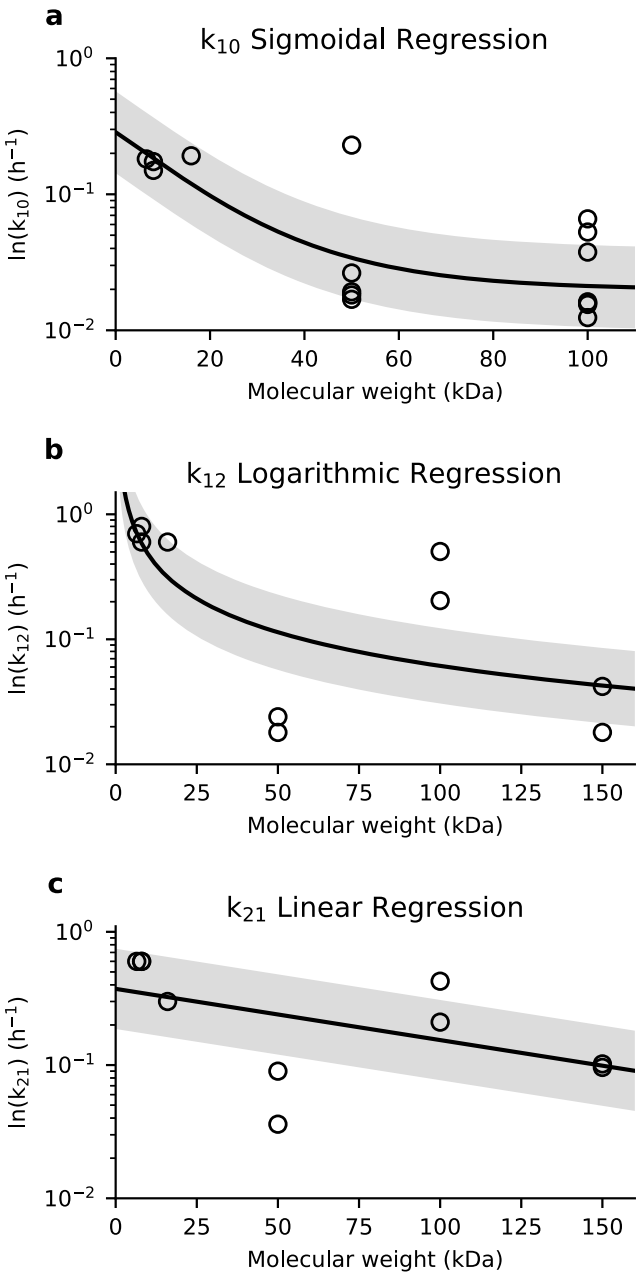


**Fig. 3.** Regressions of $k_{10}$ (a), $k_{12}$ (b), and $k_{21}$ (c) parameters against molecular weight. Parameter values were regressed against molecular weight using sigmoidal, logarithmic, and linear models, respectively. As IgGs are recycled by the FcRn system, these values were excluded from the $k_{10}$ regression. Shaded regions denote the 2-fold error envelope.

Across the different scaffolds, increasing molecular weight generally leads to a longer elimination half-life and reduced tissue perfusion. This follows the expected trend (Datta-Mannan, 2019; Li et al., 2017). The predicted Fab, $F(ab')_2$, and IgG elimination half-lives are all within their respective literature review ranges. The IgG has a markedly longer

**Table 5**
Coefficients of $k_{10}$, $k_{12}$, and $k_{21}$ parameter regression models. Coefficient letters are as referred to in the regression model equations.

| | $k_{10}$ | | | $k_{12}$ | | $k_{21}$ | |
|---|---|---|---|---|---|---|---|
| | a | b | c | a | b | a | b |
| Coefficient | 3.74 | 0.0453 | 4.92 | −0.894 | 1.32 | −0.00885 | −0.986 |
| Standard Error | 8.79 | 0.0275 | 0.398 | 0.335 | 1.27 | 0.00526 | 0.442 |

**Table 6**
Predicted pharmacokinetic parameters and dynamics of antivenom scaffolds. $k_{10}$, $k_{12}$, and $k_{21}$ rate constant values were estimated from the regression models using scaffold molecular weight. Elimination half-life and biodistribution were calculated for the simulated scaffolds.

| | | Nanobody | scFv | Fab | F (ab')$_2$ | IgG |
|---|---|---|---|---|---|---|
| Molecular weight (kDa) | | 15 | 27 | 50 | 100 | 150 |
| Parameters | $k_{10}$ ($h^{-1}$) | 0.126 | 0.0710 | 0.0341 | 0.0212 | 0.0120 |
| | $k_{12}$ ($h^{-1}$) | 0.334 | 0.198 | 0.114 | 0.0613 | 0.0426 |
| | $k_{21}$ ($h^{-1}$) | 0.327 | 0.294 | 0.240 | 0.154 | 0.0989 |
| Dynamics | T ½ $_\beta$ (h) | 12.3 | 17.4 | 31.0 | 47.1 | 84.9 |
| | BD (%) | 123 | 77.9 | 52.4 | 44 | 46.6 |

half-life than the F(ab')$_2$, indicating its FcRn recycling. Nanobodies and scFvs are known to exhibit fast and extensive tissue perfusion, and rapid elimination via the kidneys. The simulated nanobodies and scFvs do represent highly perfusive, rapidly eliminating binders, and can be used to explore the function of antivenoms which pharmacokinetically mirror the dynamics of low molecular weight toxins. The predicted half-lives of the nanobodies and scFvs are longer than those recorded in smaller animals as expected. The elimination half-life of scFvs have previously been reported as 4 h in rats and 36–48 min in mice (Hutt et al., 2012; Li et al., 2019; Schneider et al., 2016). The half-life of nanobodies has been recorded as 36 min in rats and 32 min in mice (Hoefman et al., 2015; van Faassen et al., 2020). Small antibody fragments such as nanobodies and scFvs can be PEGylated and fused to other proteins to improve their longevity, and in clinical applications this may be required (Hutt et al., 2012; Jevševar et al., 2012).

The BD was based on the biodistribution coefficient defined by Shah and Betts (2013), which refers to the ratio of a drug concentration in a designated tissue relative to the blood. Whilst our BD ratios cannot be directly compared to existing measurements due to the lumped nature of our compartments, the general trend of increasing tissue perfusion with decreasing scaffold size is in agreement with Li et al. (2016). As an additional validation step, the central compartment profiles of the IgG, F (ab')$_2$, and Fab antivenoms were simulated and compared against the literature review antivenom studies used for the regressions. The simulated profiles lay within the bounds of these reported studies (ESM Section 5: Figs. S2-S3).

### 3.4. Simulation of envenomation and antivenom treatment

Next, we simulated envenomation and treatment to explore the impact of different antivenom doses, scaffolds, and treatment delays on therapeutic outcome. For model verification, we compared our results with experimental rescue studies, in which animals are injected with venom and treated after a time delay. We simulated an intramuscular *N. sumatrana* envenomation, with treatment using high affinity Fab, F (ab')$_2$, and IgG antivenoms. *N. sumatrana* venom is dominated by low molecular weight three-finger toxins and phospholipase $A_2$s which have rapid-acting neurotoxic and cytotoxic effects (Chong et al., 2019; Yap et al., 2014a). The compartmental parameters of its whole venom were taken from a previous study (Yap et al., 2014b).

Fig. 5a–b shows a treatment scenario whereby a subtherapeutic dose of Fab antivenom is administered following a 3 mg (1.5 mg/kg) envenomation. Due to the antivenom's high binding affinity, the free venom is rapidly neutralised in the central blood compartment. The

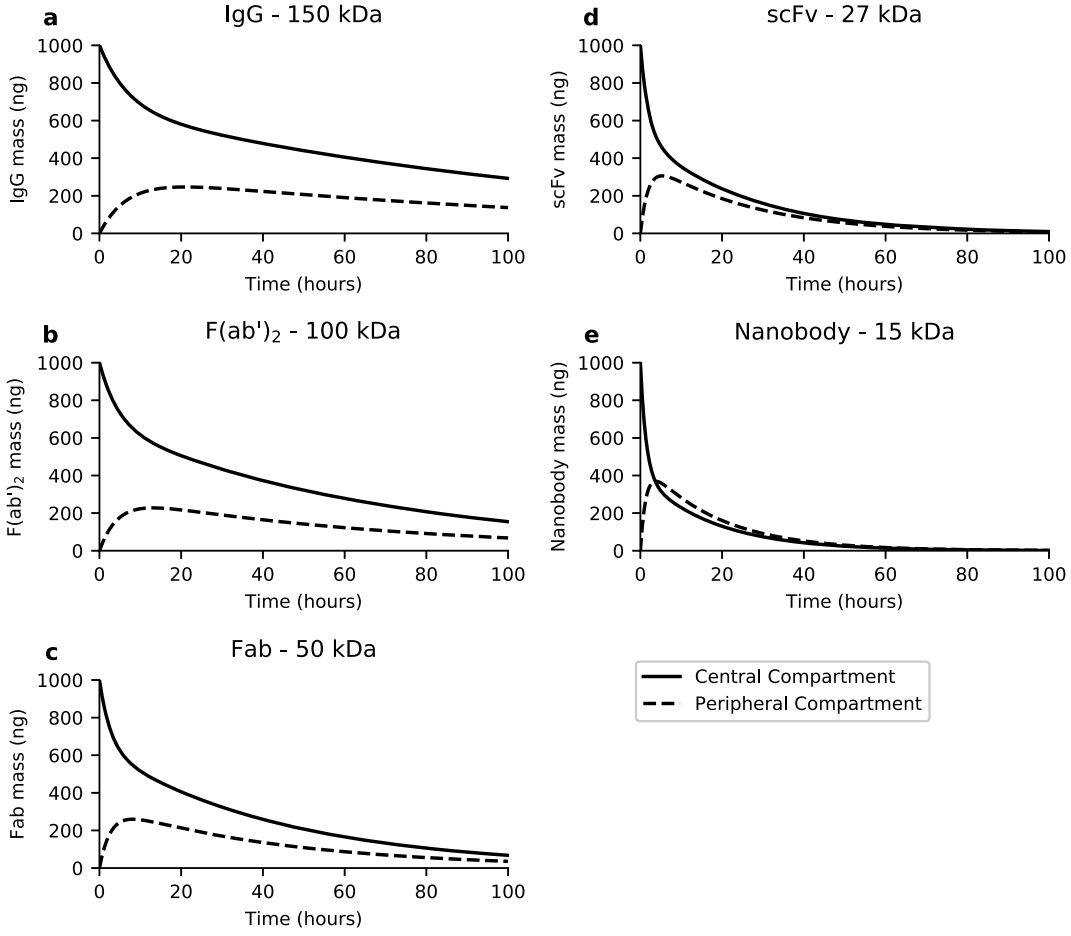


**Fig. 4.** Two-compartment simulations of IgG (a), F(ab')$_2$ (b), Fab (c), scFv (d), and nanobody (e) antivenoms using $k_{10}$, $k_{12}$, and $k_{21}$ values predicted by parameter regressions. Starting dose = 1000 ng.

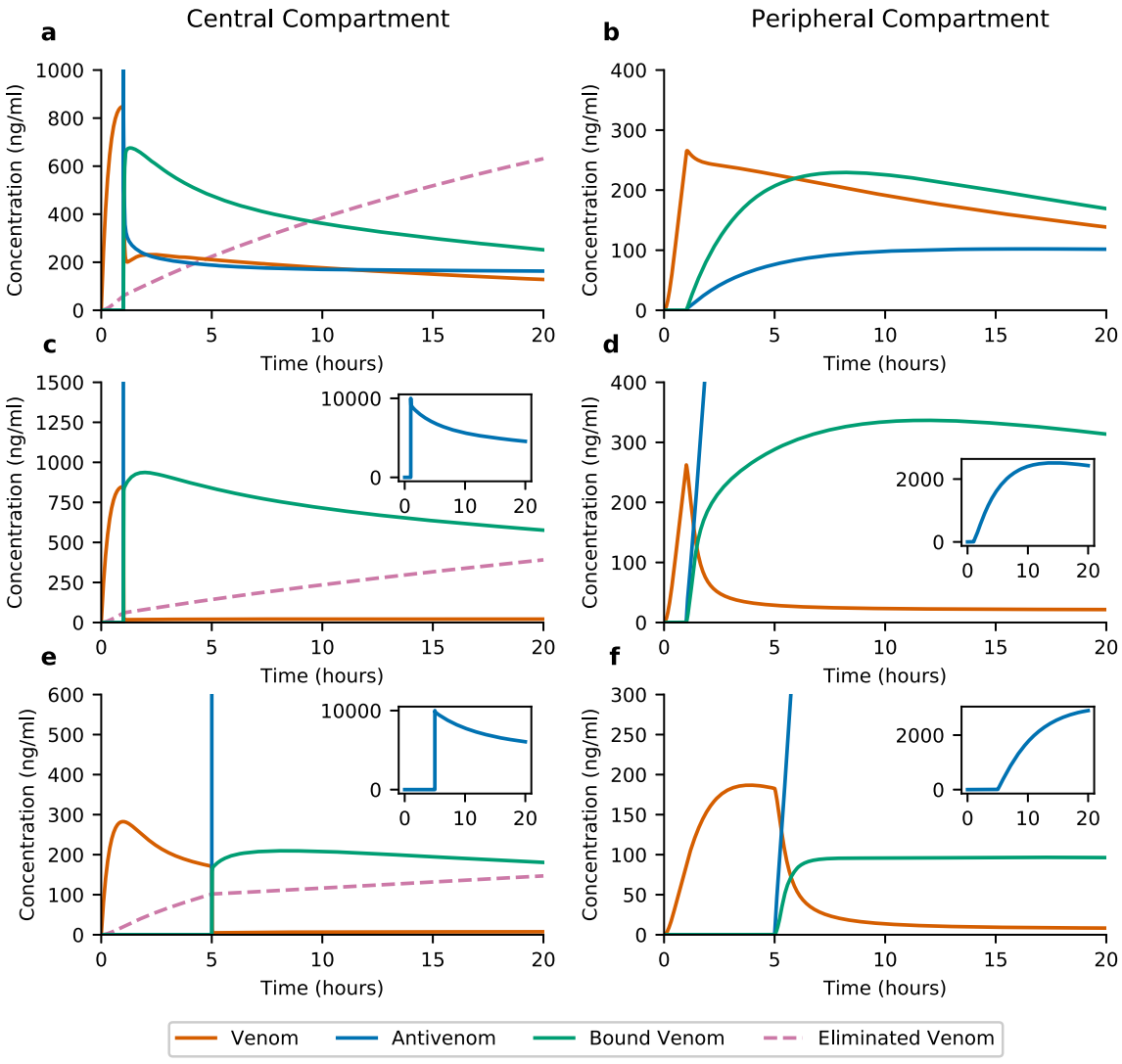


**Fig. 5.** Simulation of *N. sumatrana* venom treatment with Fab, F(ab')$_2$ and IgG antivenoms. Panels on the left-hand side show the central compartment, and panels on the right show the peripheral compartment. Inset graphs show the antivenom concentration-time curve. Panels a–b show the treatment of a 3 mg venom dose with 1 mg Fab antivenom at 1 h. Panels c–d show the treatment of a 3 mg venom dose with 10 mg F(ab')$_2$ antivenom at 1 h. Panels e–f show the treatment of a 1 mg venom dose with 10 mg IgG antivenom at 5 h. For all antivenoms, $k_{on} = 6 \times 10^5$ $M^{-1}s^{-1}$ and $k_{off} = 1 \times 10^{-3}$ $s^{-1}$ ($K_D = 1.67$ nM).

coinciding depletion of free antivenom leads to a slight resurgence in central compartment venom levels, as additional toxins continue to move from the bite site into the blood. Due to its relatively small size, the Fab antivenom quickly distributes to the peripheral tissue. Owing to the insufficient dose, the venom is incompletely neutralised, with significant venom concentrations of approximately 200 ng ml$^{-1}$ persisting across both compartments. As the concentration curves plateau the system reaches a steady state, with the relatively low circulating concentrations of free antivenom reducing the rate of venom neutralisation.

Fig. 5c–d shows a scenario whereby a larger 10 mg dose of F(ab')$_2$ antivenom is administered to treat 3 mg venom at 1 h. Antivenom saturates the system leading to the rapid and sustained decline and suppression of venom levels in both compartments. There is however a small amount of remaining venom in the peripheral compartment, which is again likely a result of a reduced neutralisation rate from the low venom concentration.

Fig. 5e–f shows a scenario whereby 10 mg IgG antivenom is administered 5 h after a 1 mg bite (0.5 mg/kg). In this case, a large amount of venom has distributed into the peripheral compartment. Due to the high levels of circulating IgG, a significant amount of antivenom moves into the peripheral tissue compartment to neutralise venom, albeit at a slower rate than the smaller F(ab')$_2$ fragment. The system is again saturated and venom levels are rapidly suppressed in both regions of the body.

Whilst the central compartment tracks more than just blood and so cannot be directly compared to experimental studies, the overall dynamics align with previous *in vivo* work. Antivenom administration in all cases leads to a sharp and rapid decline in central compartment venom concentration, mirroring the known effects of antivenom on blood venom levels (Calderón-Aranda et al., 1999; Krifi et al., 2001, 2005; Rivière et al., 1997). The simulated central compartment $C_{max}$ (maximal concentration) additionally aligns with known ranges for moderate and severe envenoming. The moderate 0.5 mg/kg envenoming case in Fig. 5e has a $C_{max}$ of 283 ng ml$^{-1}$. This is similar to the reported plasma $C_{max}$ of 392 ng ml$^{-1}$ in the original paper, which followed the same intramuscular dose (Yap et al., 2014b). The $C_{max}$ of a sub-lethal *Naja sputatrix* rabbit envenoming has also been reported in a similar range, at 447 ng ml$^{-1}$ (Yap et al., 2013). Fig. 5a and c have a $C_{max}$ of 848 ng ml$^{-1}$, indicating a more severe envenoming. The envenomation model was additionally used to simulate an existing experimental study of a scorpion envenomation with F(ab')$_2$ treatment (Krifi et al., 2001), and the model was able to recapitulate the observed neutralisation dynamics.

The results of these simulations are shown in the ESM (Section 7: Figure S5).

### 3.5. Simulations of variable venom dosing can predict effective antivenom doses

The model can be used to explore the impact of parameter variation. To quantify the impact of varying venom dose on model output, we plotted the minimum and maximum concentration-time curves over a range of venom doses. Spanning a venom dose range of 0.25–5 mg/kg, we first simulated treatment with 2.5 mg/kg $F(ab')_2$ antivenom (Fig. 6a–b). In this simulation, whilst venom in the central compartment is neutralised, there are significant levels of persistent venom in the peripheral compartment at higher venom doses. On increasing the antivenom dose to 7.5 mg/kg, venom in both compartments is rapidly and completely neutralised across the entire dose range, and there are high levels of remaining free circulating antivenom in both compartments (Fig. 6c–d). Using this approach, effective antivenom doses for a range of envenomation scenarios can be predicted. We additionally simulated the effects of varying venom bioavailability and absorption rate (ESM Section 8: Figs. S6-S8).

## 4. Discussion

### 4.1. Pharmacokinetic models have useful applications in antivenom development

In this study, we have defined a mathematical model for systemic snake envenomation and treatment. The two-compartment pharmacokinetic system aligns with the known dynamics of both snake venom and antivenom and allows for straightforward application of experimentally determined parameters. A classical two-compartment model was chosen over a physiologically-based pharmacokinetic modelling (PBPK) approach as it is simpler, easier to parameterise with existing data, and it would be readily transferable to standard pharmacokinetic studies. Whilst parameterised using rabbit data, parameters from other species could be applied to the mathematical model. The model can predict the changing concentrations of toxins, antivenoms, and neutralised toxins in two compartments over time, and indicates the extent, speed, and longevity of neutralisation.

We believe that computational pharmacokinetic models can provide a useful tool to predict and compare the function of different antivenom treatments. Whilst numerous different scaffolds have been suggested based on biological or manufacturing merit, there has been little definitive, evidence-based guidance as to the most significant pharmacokinetic factors relevant to antivenom development, beyond affinity (Alvarenga et al., 2014; Jenkins et al., 2019; Laustsen et al., 2018b). Computational simulation can help elucidate the underlying system dynamics, and we plan to undertake further comparative simulations of different scaffolds to this end. Whilst we have predicted the dynamics of different antivenoms using molecular size as a key discriminant, a better experimental understanding of the movement of different scaffolds in the body would help inform this model in the future. The pharmacokinetics and *in vivo* effectiveness of newer scaffolds particularly warrant further investigation and comparison to conventional formats. Future recombinant antivenoms would likely be formulated as oligoclonal cocktails, and utilisation of multiple different scaffold types has been speculated as a way to improve neutralisation coverage (Kini et al., 2018). Antibody cocktails can face additional challenges in manufacturing, formulation, clinical trial design, dosing, and regulation (Larbouret et al., 2021). Since these issues would likely be compounded in the development of a multi-scaffold cocktail, there should be a good evidence base to suggest that significant treatment benefits would arise from their use. Computational pharmacokinetic simulations could be applied in the future development of single and multi-scaffold antivenom cocktails, to explore the impact of various stoichiometric ratios

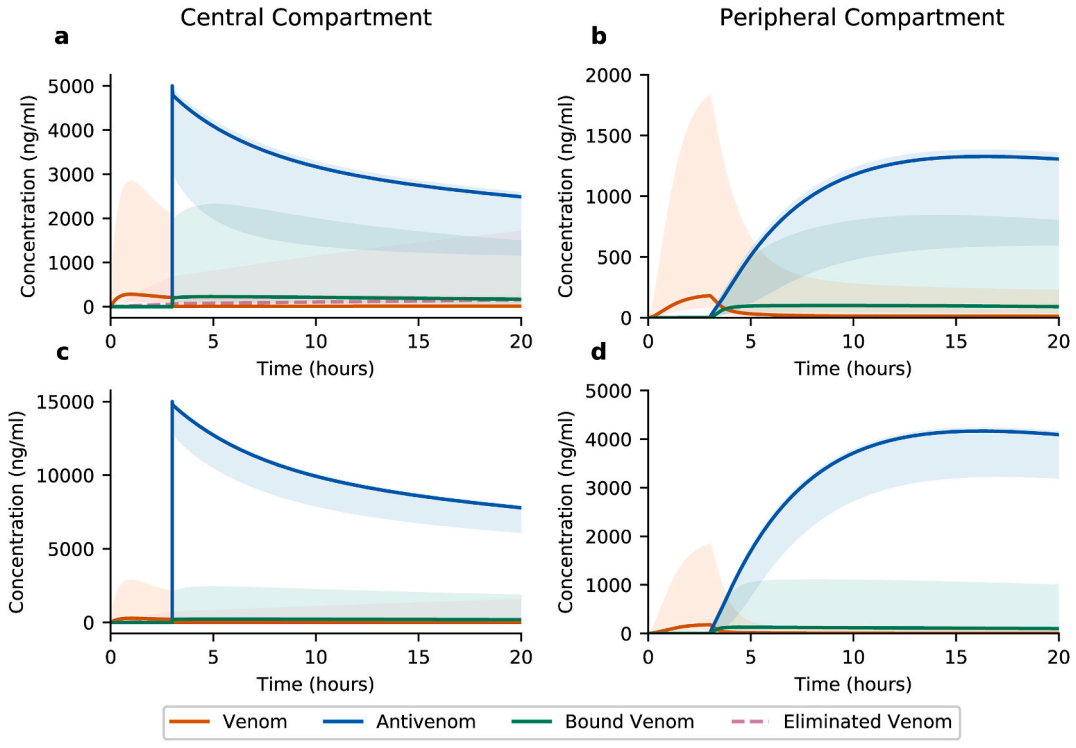


**Fig. 6.** Simulation of variable *N. sumatrana* venom doses, treated with $F(ab')_2$ antivenom. Panels on the left-hand side show the central compartment, and panels on the right show the peripheral compartment. Panels a–b show the treatment of a 0.5–10 mg venom dose with 5 mg $F(ab')_2$ antivenom at 3 h. Panels c–d show the treatment of a 0.5–10 mg venom dose with 15 mg $F(ab')_2$ antivenom at 3 h. Solid lines indicate the time series of a 1 mg venom dose baseline case. For all simulations, $k_{on} = 6 \times 10^5\ M^{-1}s^{-1}$ and $k_{off} = 1 \times 10^{-3}\ s^{-1}$ ($K_D = 1.67$ nM), and a 2 kg rabbit weight was assumed.

and scaffold combinations. Simulations can also help predict the impact of dose levels, dose timing, repeated dosing, and treatment delays, to inform the effective use of antivenoms.

### 4.2. Standardised antivenom pharmacokinetic studies would further improve our model's predictions

The model was parameterised using data from rabbit studies. To enable simulation of venoms and antivenoms of various sizes, the core $k_{10}$, $k_{12}$, and $k_{21}$ parameters were regressed against molecular weight. Molecular size is known to affect elimination pathways, capillary transport, molecular diffusion, and lymph uptake (Knauf et al., 1988; Li and Shah, 2019; Reddy et al., 2006; Sánchez-Félix et al., 2020). The regressions are however a simplification since other properties such as isoelectric point, protein shape, and plasma flow rates are also known to influence transport and elimination (Bumbaca et al., 2012; Deen et al., 1979; Sánchez-Félix et al., 2020). Despite the limited number of experimental input studies and the high variability of their parameters, the final regression predictions together produced scaffold behaviour that followed the expected trend of decreased tissue perfusion and elimination with increasing molecular weight. The $k_{12}$ regression had poor prediction efficacy which casts doubt as to the validity of the simulated antivenom tissue perfusion. We were unable to find previous work correlating the $k_{12}$ and $k_{21}$ rates with molecular size, and so it is difficult to say exactly what these relationships should look like. It is pertinent to note that several studies relied on radioimmunoassay (RIA) to track antivenom blood concentrations instead of enzyme-linked immunoassay (ELISA). Discrepancies between RIA and ELISA measurements of antivenoms have previously been described, with RIA having been found to overestimate antivenom concentration, potentially by detecting degraded antibodies (Krifi et al., 2005). The only studies which supplied antivenom compartmental transfer rates were measured by RIA, and so whilst these were included in the regressions, these values may be less reliable. Low molecular weight toxins were also included in the regressions to enable simulation of low molecular weight antivenoms in the absence of existing data for these scaffolds in rabbits. Whilst none of the toxins were recorded as exhibiting target mediated drug disposition (TMDD), if any of the toxins exhibited modified pharmacokinetics due their toxic activity, this may have biased the regressions. None of the antivenoms reported TMDD. In the future, controlled and standardised studies to calculate and compare the $k_{10}$, $k_{12}$ and $k_{21}$ rates for antivenoms of various sizes could better inform these relationships and improve our model's predictions.

### 4.3. Simulations indicate that targeted recombinant antivenoms could substantially lower effective dose requirements

The *N. sumatrana* envenomation treatment simulations recapitulate experimentally observed dynamics, and can be used to project therapeutic dose levels for different envenomation scenarios. Since our model assumes that there are no extraneous antivenom binders, the simulations highlight the dose reduction benefits that could result from recombinant antivenom use. Previously, for treatment of 0.1 mg/kg scorpion venom in rabbits, the minimal effective $F(ab')_2$ antivenom doses have ranged from 6 to 12 mg/kg (Krifi et al., 2001, 2005). In our simulations, 5 mg/kg antivenom can neutralise a higher venom dose of 1.5 mg/kg, demonstrating a far higher therapeutic potency. *N. sumatrana* itself does not have a specific antivenom, however the efficacy of the polyvalent Haffkine antivenom which targets a related species has previously been investigated. Efficacy studies found that the $ED_{50}$ of the Haffkine antivenom against an intravenous 2.5 $LD_{50}$ venom dose (1.25 mg/kg) in mice was 73.9 mg (Cham et al., 2013). This is drastically higher than our effective simulation doses of 10 mg. Two additional heterologous antivenoms, Serum Anti Ular Bisa (SABU) and Thai Neuro Polyvalent Antivenom (NPAV), have also been efficacy tested with *N. sumatrana* venom. The normalised potency (the mg of venom which are neutralised per g of antivenom protein) against *N. sumatrana* venom was 1.8 mg/g for SABU, and 7.1 mg/g for NPAV (Tan et al., 2016a, 2016b). In our 2 kg rabbit model, an IM venom dose of 3 mg with 41.9% bioavailability translates to roughly 1.26 mg venom in circulation. Based on these potencies, 700 mg of SABU and 177 mg NPAV would be required to neutralise a 1.26 mg intravenous venom dose, which is again far higher than our simulated 10 mg treatment dose. The normalised potencies of SABU and NPAV against one of their target species *N. sputatrix* are 2.9 mg/g and 8.3 mg/g, respectively, which still translates to high treatment doses (Tan et al., 2016a, 2016b). Testing the effect of variability in the injected venom dose provides a useful tool to elucidate therapeutic antivenom dose ranges. We screened a large venom dose range of 0.25 – 5 mg/kg. Whilst at the upper levels of this range a 2.5 mg/kg $F(ab')_2$ antivenom dose was unable to completely neutralise the venom, a moderate increase to 7.5 mg/kg provided full protection. This dose again compares favourably with the previously mentioned antivenoms.

It is worth noting that our model simulates a monovalent antivenom: the antivenoms mentioned here may have lower proportions of neutralising binders due to their polyvalency. Previously a monovalent *N. kaouthia* antivenom was found to have a higher normalised potency of 20.44 mg/g (Tan et al., 2016a, 2016b). However, comparative studies have also found that polyvalent antivenoms can be prepared with comparable potencies to their monovalent counterparts, and so large potency increases may not always be achieved through monovalent manufacture (Raweerith and Ratanabanangkoon, 2005).

Poor antivenom potency is a pressing issue, with the reported proportions of therapeutically active binders within serum antivenoms ranging from 5% to 36% (Laustsen et al., 2017). Serum-based elapid antivenoms are typically less potent than viper antivenoms, due to the poor immunogenicity of the small neurotoxins which typically dominate their venom. Treatment of severe cases can therefore require a large dose of antivenom (Leong et al., 2015; Ratanabanangkoon, 2021). *In vitro* selection techniques can enable the discovery of antibodies against poorly immunogenic targets (Chan et al., 2014). Such methods have already successfully yielded high affinity recombinant binders against small elapid toxins (Laustsen et al., 2018a; Ledsgaard et al., 2021; Richard et al., 2013). Antibodies selected through these means could be used in recombinant formulations for high-potency antivenoms. As our simulations demonstrate, targeted recombinant antivenoms could substantially lower effective dose requirements. Given that the model does not account for the variable protein toxicities and synergism within venom, it likely overestimates the dose of recombinant antivenom that would be required for treatment.

### 4.4. Model limitations and future expansions

The model design does come with limitations. Since the central compartment contains multiple tissues, blood concentrations cannot be directly predicted from this model. The model also does not reproduce the venom redistribution dynamics seen in experimental insufficient dose cases, whereby venom moves down a concentration gradient from the tissue to the blood to cause a large resurgence in plasma venom levels (Calderón-Aranda et al., 1999; Krifi et al., 2001, 2005). This is likely due to the inclusion of rapidly equilibrating tissues in the central compartment of our model, which would predominantly contribute to this resurgence. To simulate this effect, one would need to model the blood separately from the well-perfused tissues. The dynamics of the neutralised toxins are also assumed. Since *N. sumatrana* venom is dominated by low molecular weight (<20 kDa) toxins, we assumed that the toxin-venom complexes would take on the pharmacokinetic parameters of the antivenoms which are much larger in size. In simulations involving smaller scaffolds or larger toxins, the dynamics of the neutralised population could be estimated using the regression relationships defined within this study.

Whilst *N. sumatrana* venom can be simulated quite simply, venoms with a greater molecular weight spread may require a more complex

model. Viper venoms for example typically have a more complex, prolonged absorption profile due to their toxin composition. Encapsulation of these dynamics may require parallel simulation of toxin subpopulations at different molecular weights. The model is also unable to predict local venom effects. *N. sumatrana* venom has a limited bioavailability of 42%, indicating a substantial accumulation of the venom at the bite site where it is known to cause tissue damage (Yap et al., 2014b). A higher bioavailability may indicate more severe systemic effects of the venom. Local tissue damage could be simulated using a spatialised stochastic model, whereby venom and antivenom particles are individually tracked as they diffuse through tissue. Such techniques have been applied to the design of cancer-targeting nanoparticles, and could be adapted to inform the development of localised envenomation therapies (Stillman et al., 2020). Spatialised simulations could also be used to address our model's assumption that the venom and antivenom compartmental volumes of distribution are equivalent and overlapping, which is unlikely to be the case in real life. Local tissue damage could alternatively be incorporated into the current model by simulating the venom depot site as a third compartment. This would require the quantification of the rates of venom and antivenom transfer in and out of the bite site.

The model was validated using comparisons to existing pharmacokinetic studies of antivenoms, and envenomation rescue experiment studies. These comparisons were limited by the high variability of existing antivenom data, and the scarcity of pharmacokinetic studies on envenomation treatment. To further validate the model, pharmacokinetic profiles of antivenoms and venoms would be required to generate the compartmental parameters for model initialisation. Measured profiles of both venom and antivenom in the treatment case could then be compared against model predictions.

Finally, the model is parameterised using rabbit data. This currently represents the largest source of pharmacokinetic data on venoms and antivenoms, and gives distinct benefits to model validation. To apply the model to humans, values for the $k_{10}$, $k_{12}$, and $k_{21}$ parameters of antivenoms and venoms would be required. Whilst controlled trials could be established for antivenoms to obtain these values, it is more difficult to calculate reliable parameters for venoms in humans due to toxicological study limitations. These parameters could be approximated using pharmacokinetic data from similarly sized proteins, however one would need to be mindful of the potential for altered venom disposition due to toxin function. As an alternative, parameters could be allometrically scaled from animals to humans. In this, an exponential equation is used to scale parameters between species of different body weights. Whilst scaling for some parameters such as clearance is well-established, on review of the literature there was no consensus as to the best scaling exponent for the $k_{10}/k_{12}/k_{21}$ parameters. We have found studies using exponents of −0.15, 0.25 and 0.75, a large range which would have a big impact on the resulting predictions (Luu et al., 2012; Nakamura et al., 2020; Wang et al., 2016). To reliably perform scaling, one may need to calculate the scaling constant or otherwise assess its applicability.

## 5. Conclusions

In summary, we have developed an *in silico* model of systemic snakebite envenomation and treatment. We have identified relationships between molecular size and key pharmacokinetic parameters to enable the comparative simulation of antivenoms of diverse molecular formats. Our case study of simulated treatment of *N. sumatrana* envenomation has underscored the drastic dose reductions that could result from future adoption of recombinant antivenoms. This model system could be used to compare the utility of current and next-generation antivenom scaffolds against a variety of venoms in clinically relevant treatment scenarios.

## Statements and declarations

The authors have no relevant financial or non-financial interests to declare.

## Funding

N.M.M would like to acknowledge funding from the Engineering and Physical Sciences Research Council (EPSRC) grant number EP/L016494/1. S.H and J.A.B were funded by EU Horizon 2020 (grant number 800983) and Cancer Research UK (grant number C18281/A29019).

## Ethical statement

This research was conducted according to the ethical guidelines of Toxicon. All authors have meaningfully contributed to this article. The manuscript reflects the authors own original works and credits its sources appropriately. This paper is not currently being considered for publication elsewhere.

## Declaration of competing interest

The authors declare that they have no known competing financial interests or personal relationships that could have appeared to influence the work reported in this paper.

## Appendix A. Supplementary data

Supplementary data to this article can be found online at https://doi.org/10.1016/j.toxicon.2022.06.006.

## References

Alvarenga, L.M., Zahid, M., Tommaso, A.D., Juste, M.O., Aubrey, N., Billiald, P., Muzard, J., 2014. Engineering venom's toxin-neutralizing antibody fragments and its therapeutic potential. Toxins 6, 2541–2567. https://doi.org/10.3390/toxins6082541.

Bates, A., Power, C.A., 2019. David vs. Goliath: the structure, function, and clinical prospects of antibody fragments. Antibodies 8, 28. https://doi.org/10.3390/antib8020028.

Bazin-Redureau, M., Pepin, S., Hong, G., Debray, M., Scherrmann, J.M., 1998. Interspecies scaling of clearance and volume of distribution for horse antivenom F (ab')2. Toxicol. Appl. Pharmacol. 150, 295–300. https://doi.org/10.1006/taap.1997.8363.

Boels, D., Hamel, J.F., Le Roux, G., Labadie, M., Paret, N., Delcourt, N., Langrand, J., Puskarczyk, E., Nisse, P., Sinno-Tellier, S., de Haro, L., 2020. Snake bites by European vipers in Mainland France in 2017-2018: comparison of two antivenoms Viperfav® and Viperatab®. Clin. Toxicol. 58, 1050–1057. https://doi.org/10.1080/15563650.2020.1726377.

Boxenbaum, H., 1982. Interspecies scaling, allometry, physiological time, and the ground plan of pharmacokinetics. J. Pharmacokinet. Biopharm. 10, 201–227. https://doi.org/10.1007/BF01062336.

Boyer, L.V., Seifert, S.A., Clark, R.F., McNally, J.T., Williams, S.R., Nordt, S.P., Walter, F. G., Dart, R.C., 1999. Recurrent and persistent coagulopathy following pit viper envenomation. Arch. Intern. Med. 159, 706–710. https://doi.org/10.1001/archinte.159.7.706.

Bumbaca, D., Boswell, C.A., Fielder, P.J., Khawli, L.A., 2012. Physiochemical and biochemical factors influencing the pharmacokinetics of antibody therapeutics. AAPS J. 14, 554–558. https://doi.org/10.1208/s12248-012-9369-y.

Bush, S.P., Ruha, A.-M., Seifert, S.A., Morgan, D.L., Lewis, B.J., Arnold, T.C., Clark, R.F., Meggs, W.J., Toschlog, E.A., Borron, S.W., Figge, G.R., Sollee, D.R., Shirazi, F.M., Wolk, R., de Chazal, I., Quan, D., García-Ubbelohde, W., Alagón, A., Gerkin, R.D., Boyer, L.V., 2015. Comparison of F(ab')2 versus Fab antivenom for pit viper envenomation: a prospective, blinded, multicenter, randomized clinical trial. Clin. Toxicol. 53, 37–45. https://doi.org/10.3109/15563650.2014.974263.

Calderón-Aranda, E.S., Rivière, G., Choumet, V., Possani, L.D., Bon, C., 1999. Pharmacokinetics of the toxic fraction of Centruroides limpidus limpidus venom in experimentally envenomed rabbits and effects of immunotherapy with specific F (ab')2. Toxicon 37, 771–782. https://doi.org/10.1016/S0041-0101(98)00216-5.

Carotenuto, S.E., Bergman, P.J., Ray, J.R., McKee, T., 2021. Retrospective comparison of three antivenoms for the treatment of dogs with crotalid envenomation. J. Am. Vet. Med. Assoc. 259, 503–509. https://doi.org/10.2460/javma.259.5.503.

Casewell, N.R., Jackson, T.N.W., Laustsen, A.H., Sunagar, K., 2020. Causes and consequences of snake venom variation. Trends Pharmacol. Sci. 41, 570–581. https://doi.org/10.1016/j.tips.2020.05.006.

Cham, G., Lim, F., Earnest, A., Gopalakrishnakone, P., 2013. Cross-Reactivity against Naja sumatrana (black spitting cobra) envenoming from the haffkine antivenom in a mouse model. ISRN Toxicol. 1–5. https://doi.org/10.1155/2013/247645, 2013.
Chan, C.E.Z., Lim, A.P.C., MacAry, P.A., Hanson, B.J., 2014. The role of phage display in therapeutic antibody discovery. Int. Immunol. 26, 649–657. https://doi.org/10.1093/intimm/dxu082.
Chong, H.P., Tan, K.Y., Tan, N.H., Tan, C.H., 2019. Exploring the diversity and novelty of toxin genes in Naja sumatrana, the equatorial spitting cobra from Malaysia through de Novo venom-Gland transcriptomics. Toxins 11, E104. https://doi.org/10.3390/toxins11020104.
Dart, R.C., McNally, J., 2001. Efficacy, safety, and use of snake antivenoms in the United States. Ann. Emerg. Med. 37, 181–188. https://doi.org/10.1067/mem.2001.113372.
Datta-Mannan, A., 2019. Mechanisms influencing the pharmacokinetics and disposition of monoclonal antibodies and peptides. Drug Metab. Dispos. 47, 1100–1110. https://doi.org/10.1124/dmd.119.086488.
de Silva, H.A., Ryan, N.M., de Silva, H.J., 2016. Adverse reactions to snake antivenom, and their prevention and treatment. Br. J. Clin. Pharmacol. 81, 446–452. https://doi.org/10.1111/bcp.12739.
Deen, W.M., Bohrer, M.P., Brenner, B.M., 1979. Macromolecule transport across glomerular capillaries: application of pore theory. Kidney Int. 16, 353–365. https://doi.org/10.1038/ki.1979.138.
El Hafny, B., Chgoury, F., Adil, N., Cohen, N., Hassar, M., 2002. Intraspecific variability and pharmacokinetic characteristics of Androctonus mauretanicus mauretanicus scorpion venom. Toxicon 40, 1609–1616. https://doi.org/10.1016/S0041-0101(02)00178-2.
Flanagan, R.J., Jones, A.L., 2004. Fab antibody fragments: some applications in clinical toxicology. Drug Saf. 27, 1115–1133. https://doi.org/10.2165/00002018-200427140-00004.
Gerardo, C.J., Keyler, D.E., Rapp-Olson, M., Dart, R.C., 2021. Control of venom-induced tissue injury in copperhead snakebite patients: a post hoc sub-group analysis of a clinical trial comparing F(ab')2 to Fab antivenom. Clin. Toxicol. 1–3. https://doi.org/10.1080/15563650.2021.1973489.
Gutiérrez, J.M., Calvete, J.J., Habib, A.G., Harrison, R.A., Williams, D.J., Warrell, D.A., 2017. Snakebite envenoming. Nat. Rev. Dis. Prim. 3, 17063 https://doi.org/10.1038/nrdp.2017.63.
Gutiérrez, J.M., León, G., Lomonte, B., 2003. Pharmacokinetic-pharmacodynamic relationships of immunoglobulin therapy for envenomation. Clin. Pharmacokinet. 42, 721–741. https://doi.org/10.2165/00003088-200342080-00002.
Hamers-Casterman, C., Atarhouch, T., Muyldermans, S., Robinson, G., Hammers, C., Songa, E.B., Bendahman, N., Hammers, R., 1993. Naturally occurring antibodies devoid of light chains. Nature 363, 446–448. https://doi.org/10.1038/363446a0.
Herrera, M., Sánchez, M., Machado, A., Ramírez, N., Vargas, M., Villalta, M., Sánchez, A., Segura, Á., Gómez, A., Solano, G., Gutiérrez, J.M., León, G., 2017. Effect of premedication with subcutaneous adrenaline on the pharmacokinetics and immunogenicity of equine whole IgG antivenom in a rabbit model. Biomed. Pharmacother. 90, 740–743. https://doi.org/10.1016/j.biopha.2017.04.039.
Hoefman, S., Ottevaere, I., Baumeister, J., Sargentini-Maier, M.L., 2015. Pre-clinical intravenous serum pharmacokinetics of albumin binding and non-half-life extended nanobodies. Antibodies 4, 141–156. https://doi.org/10.3390/antib4030141.
Hutt, M., Färber-Schwarz, A., Unverdorben, F., Richter, F., Kontermann, R.E., 2012. Plasma half-life extension of small recombinant antibodies by fusion to immunoglobulin-binding domains *. J. Biol. Chem. 287, 4462–4469. https://doi.org/10.1074/jbc.M111.311522.
Ismail, M., Abd-Elsalam, M.A., 1998. Pharmacokinetics of 125I-labelled IgG, F(ab')2 and Fab fractions of scorpion and snake antivenins: merits and potential for therapeutic use. Toxicon 36, 1523–1528. https://doi.org/10.1016/S0041-0101(98)00144-5.
Ismail, M., Abd-Elsalam, M.A., Al-Ahaidib, M.S., 1998. Pharmacokinetics of 125I-labelled Walterinnesia aegyptia venom and its specific antivenins: flash absorption and distribution of the venom and its toxin versus slow absorption and distribution of IgG, F(ab')2 and F(ab) of the antivenin. Toxicon 36, 93–114. https://doi.org/10.1016/S0041-0101(97)00062-7.
Ismail, M., Aly, M.H.M., Abd-Elsalam, M.A., Morad, A.M., 1996. A three-compartment open pharmacokinetic model can explain variable toxicities of cobra venoms and their alpha toxins. Toxicon 34, 1011–1026. https://doi.org/10.1016/0041-0101(96)00055-4.
Jenkins, T.P., Fryer, T., Dehli, R.I., Jürgensen, J.A., Fuglsang-Madsen, A., Føns, S., Laustsen, A.H., 2019. Toxin neutralization using alternative binding proteins. Toxins 11, 53. https://doi.org/10.3390/toxins11010053.
Jenkins, T.P., Laustsen, A.H., 2020. Cost of manufacturing for recombinant snakebite antivenoms. Front. Bioeng. Biotechnol. 8 https://doi.org/10.3389/fbioe.2020.00703.
Jevševar, S., Kusterle, M., Kenig, M., 2012. PEGylation of antibody fragments for half-life extension. In: Proetzel, G., Ebersbach, H. (Eds.), Antibody Methods and Protocols, Methods in Molecular Biology. Humana Press, Totowa, NJ, pp. 233–246. https://doi.org/10.1007/978-1-61779-931-0_15.
Johanson, G., 2010. 1.08 - modeling of disposition. In: McQueen, C.A. (Ed.), Comprehensive Toxicology, second ed. Elsevier, Oxford, pp. 153–177. https://doi.org/10.1016/B978-0-08-046884-6.00108-1.
Kini, R.M., Doley, R., 2010. Structure, function and evolution of three-finger toxins: mini proteins with multiple targets. Toxicon 56, 855–867. https://doi.org/10.1016/j.toxicon.2010.07.010.
Kini, R.M., Sidhu, S.S., Laustsen, A.H., 2018. Biosynthetic oligoclonal antivenom (BOA) for snakebite and next-generation treatments for snakebite victims. Toxins 10, 534. https://doi.org/10.3390/toxins10120534.
Knauf, M.J., Bell, D.P., Hirtzer, P., Luo, Z.P., Young, J.D., Katre, N.V., 1988. Relationship of effective molecular size to systemic clearance in rats of recombinant interleukin-2 chemically modified with water-soluble polymers. J. Biol. Chem. 263, 15064–15070. https://doi.org/10.1016/S0021-9258(18)68146-3.
Krifi, M.N., Miled, K., Abderrazek, M., El Ayeb, M., 2001. Effects of antivenom on Buthus occitanus tunetanus (Bot) scorpion venom pharmacokinetics: towards an optimization of antivenom immunotherapy in a rabbit model. Toxicon 39, 1317–1326. https://doi.org/10.1016/S0041-0101(01)00083-6.
Krifi, M.N., Savin, S., Debray, M., Bon, C., El Ayeb, M., Choumet, V., 2005. Pharmacokinetic studies of scorpion venom before and after antivenom immunotherapy. Toxicon 45, 187–198. https://doi.org/10.1016/j.toxicon.2004.10.007.
Larbouret, C., Gros, L., Pèlegrin, A., Chardès, T., 2021. Improving biologics' effectiveness in clinical oncology: from the combination of two monoclonal antibodies to oligoclonal antibody mixtures. Cancers 13, 4620. https://doi.org/10.3390/cancers13184620.
Laustsen, A.H., 2016. Toxin synergism in snake venoms. Toxin Rev. 35, 165–170. https://doi.org/10.1080/15569543.2016.1220397.
Laustsen, A.H., Johansen, K.H., Engmark, M., Andersen, M.R., 2017. Recombinant snakebite antivenoms: a cost-competitive solution to a neglected tropical disease? PLoS Neglected Trop. Dis. 11, e0005361 https://doi.org/10.1371/journal.pntd.0005361.
Laustsen, A.H., Karatt-Vellatt, A., Masters, E.W., Arias, A.S., Pus, U., Knudsen, C., Oscoz, S., Slavny, P., Griffiths, D.T., Luther, A.M., Leah, R.A., Lindholm, M., Lomonte, B., Gutiérrez, J.M., McCafferty, J., 2018a. In vivo neutralization of dendrotoxin-mediated neurotoxicity of black mamba venom by oligoclonal human IgG antibodies. Nat. Commun. 9, 3928. https://doi.org/10.1038/s41467-018-06086-4.
Laustsen, A.H., María Gutiérrez, J., Knudsen, C., Johansen, K.H., Bermúdez-Méndez, E., Cerni, F.A., Jürgensen, J.A., Ledsgaard, L., Martos-Esteban, A., Øhlenschlæger, M., Pus, U., Andersen, M.R., Lomonte, B., Engmark, M., Pucca, M.B., 2018b. Pros and cons of different therapeutic antibody formats for recombinant antivenom development. Toxicon 146, 151–175. https://doi.org/10.1016/j.toxicon.2018.03.004.
Ledsgaard, L., Laustsen, A.H., Pus, U., Wade, J., Villar, P., Boddum, K., Slavny, P., Masters, E.W., Arias, A.S., Oscoz, S., Griffiths, D.T., Luther, A.M., Lindholm, M., Leah, R.A., Møller, M.S., Ali, H., McCafferty, J., Lomonte, B., Gutiérrez, J.M., Karatt-Vellatt, A., 2021. In Vitro Discovery and Optimization of a Human Monoclonal Antibody that Neutralizes Neurotoxicity and Lethality of Cobra Snake Venom. https://doi.org/10.1101/2021.09.07.459075.
León, G., Monge, M., Rojas, E., Lomonte, B., Gutiérrez, J.M., 2001. Comparison between IgG and F(ab')2 polyvalent antivenoms: neutralization of systemic effects induced by Bothrops asper venom in mice, extravasation to muscle tissue, and potential for induction of adverse reactions. Toxicon 39, 793–801. https://doi.org/10.1016/S0041-0101(00)00209-9.
León, G., Vargas, M., Segura, A., Herrera, M., Villalta, M., Sánchez, A., Solano, G., Gómez, A., Sánchez, M., Estrada, R., Gutiérrez, J.M., 2018. Current technology for the industrial manufacture of snake antivenoms. Toxicon 151, 63–73. https://doi.org/10.1016/j.toxicon.2018.06.084.
Leong, P.K., Fung, S.Y., Tan, C.H., Sim, S.M., Tan, N.H., 2015. Immunological cross-reactivity and neutralization of the principal toxins of Naja sumatrana and related cobra venoms by a Thai polyvalent antivenom (Neuro Polyvalent Snake Antivenom). Acta Trop. 149, 86–93. https://doi.org/10.1016/j.actatropica.2015.05.020.
Li, J., Zhang, H., Liu, J., Xu, K., 2006. Novel genes encoding six kinds of three-finger toxins in Ophiophagus hannah (king cobra) and function characterization of two recombinant long-chain neurotoxins. Biochem. J. 398, 233–242. https://doi.org/10.1042/BJ20060004.
Li, Z., Krippendorff, B.-F., Shah, D.K., 2017. Influence of molecular size on the clearance of antibody fragments. Pharm. Res. (N. Y.) 34, 2131–2141. https://doi.org/10.1007/s11095-017-2219-y.
Li, Z., Krippendorff, B.-F., Sharma, S., Walz, A.C., Lavé, T., Shah, D.K., 2016. Influence of molecular size on tissue distribution of antibody fragments. mAbs 8, 113–119. https://doi.org/10.1080/19420862.2015.1111497.
Li, Z., Li, Y., Chang, H.-P., Chang, H.-Y., Guo, L., Shah, D.K., 2019. Effect of size on solid tumor disposition of protein therapeutics. Drug Metab. Dispos. 47, 1136–1145. https://doi.org/10.1124/dmd.119.087809.
Li, Z., Shah, D.K., 2019. Two-pore physiologically based pharmacokinetic model with de Novo derived parameters for predicting plasma PK of different size protein therapeutics. J. Pharmacokinet. Pharmacodyn. 46, 305–318. https://doi.org/10.1007/s10928-019-09639-2.
Luu, K.T., Bergqvist, S., Chen, E., Hu-Lowe, D., Kraynov, E., 2012. A model-based approach to predicting the human pharmacokinetics of a monoclonal antibody exhibiting target-mediated drug disposition. J. Pharmacol. Exp. Therapeut. 341, 702–708. https://doi.org/10.1124/jpet.112.191999.
Mankarious, S., Lee, M., Fischer, S., Pyun, K.H., Ochs, H.D., Oxelius, V.A., Wedgwood, R. J., 1988. The half-lives of IgG subclasses and specific antibodies in patients with primary immunodeficiency who are receiving intravenously administered immunoglobulin. J. Lab. Clin. Med. 112, 634–640.
Mascarenas, D.N., Fullerton, L., Smolinske, S.C., Warrick, B.J., Seifert, S.A., 2020. Comparison of F(ab')2 and Fab antivenoms in rattlesnake envenomation: first year's post-marketing experience with F(ab')2 in New Mexico. Toxicon 186, 42–45. https://doi.org/10.1016/j.toxicon.2020.08.002.
Morais, J.F., de Freitas, M.C., Yamaguchi, I.K., dos Santos, M.C., da Silva, W.D., 1994. Snake antivenoms from hyperimmunized horses: comparison of the antivenom activity and biological properties of their whole IgG and F(ab')2 fragments. Toxicon 32, 725–734. https://doi.org/10.1016/0041-0101(94)90341-7.
Nakamura, G., Ozeki, K., Nagayasu, M., Nambu, T., Nemoto, T., Hosoya, K.-I., 2020. Predicting method for the human plasma concentration-time profile of a monoclonal

antibody from the half-life of non-human primates. Biol. Pharm. Bull. 43, 823–830. https://doi.org/10.1248/bpb.b19-01042.
Navarro, D., Vargas, M., Herrera, M., Segura, Á., Gómez, A., Villalta, M., Ramírez, N., Williams, D., Gutiérrez, J.M., León, G., 2016. Development of a chicken-derived antivenom against the taipan snake (Oxyuranus scutellatus) venom and comparison with an equine antivenom. Toxicon 120, 1–8. https://doi.org/10.1016/j.toxicon.2016.06.018.
Ober, R.J., Martinez, C., Vaccaro, C., Zhou, J., Ward, E.S., 2004. Visualizing the site and dynamics of IgG salvage by the MHC class I-related receptor, FcRn. J. Immunol. 172, 2021–2029. https://doi.org/10.4049/jimmunol.172.4.2021.
Olaoba, O.T., Karina dos Santos, P., Selistre-de-Araujo, H.S., Ferreira de Souza, D.H., 2020. Snake venom metalloproteinases (SVMPs): a structure-function update. Toxicon X 7, 100052. https://doi.org/10.1016/j.toxcx.2020.100052.
Pépin-Covatta, S., Lutsch, C., Grandgeorgefi, M., Lang, J., Scherrmann, J.-M., 1996. Immunoreactivity and pharmacokinetics of horse anti-scorpion venom F(ab')2-scorpion venom interactions. Toxicol. Appl. Pharmacol. 141, 272–277. https://doi.org/10.1016/S0041-008X(96)80033-0.
Quesada, L., Sevcik, C., Lomonte, B., Rojas, E., Gutiérrez, J.M., 2006. Pharmacokinetics of whole IgG equine antivenom: comparison between normal and envenomed rabbits. Toxicon 48, 255–263. https://doi.org/10.1016/j.toxicon.2006.05.010.
Ratanabanangkoon, K., 2021. A quest for a universal plasma-derived antivenom against all elapid neurotoxic snake venoms. Front. Immunol. 12, 1363. https://doi.org/10.3389/fimmu.2021.668328.
Raweerith, R., Ratanabanangkoon, K., 2005. Immunochemical and biochemical comparisons of equine monovalent and polyvalent snake antivenoms. Toxicon 45, 369–375. https://doi.org/10.1016/j.toxicon.2004.10.019.
Reddy, S.T., Berk, D.A., Jain, R.K., Swartz, M.A., 2006. A sensitive in vivo model for quantifying interstitial convective transport of injected macromolecules and nanoparticles. J. Appl. Physiol. 101, 1162–1169. https://doi.org/10.1152/japplphysiol.00389.2006.
Richard, G., Meyers, A.J., McLean, M.D., Arbabi-Ghahroudi, M., MacKenzie, R., Hall, J. C., 2013. In vivo neutralization of α-cobratoxin with high-affinity llama single-domain antibodies (VHHs) and a VHH-Fc antibody. PLoS One 8, e69495. https://doi.org/10.1371/journal.pone.0069495.
Rivière, G., Choumet, V., Audebert, F., Sabouraud, A., Debray, M., Scherrmann, J.-M., Bon, C., 1997. Effect of antivenom on venom pharmacokinetics in experimentally envenomed rabbits: toward an optimization of antivenom therapy. J. Pharmacol. Exp. Therapeut. 281, 1–8.
Rojas, A., Vargas, M., Ramírez, N., Estrada, R., Segura, Á., Herrera, M., Villalta, M., Gómez, A., Gutiérrez, J.M., León, G., 2013. Role of the animal model on the pharmacokinetics of equine-derived antivenoms. Toxicon 70, 9–14. https://doi.org/10.1016/j.toxicon.2013.03.013.
Roncolato, E.C., Campos, L.B., Pessenda, G., Costa e Silva, L., Furtado, G.P., Barbosa, J. E., 2015. Phage display as a novel promising antivenom therapy: a review. Toxicon 93, 79–84. https://doi.org/10.1016/j.toxicon.2014.11.001.
Rowland, M., Tozer, T.N., 1995. Clinical Pharmacokinetics Concepts and Applications, third ed. Lippincott Williams & Wilkins, Philadephia, USA.
Sánchez-Félix, M., Burke, M., Chen, H.H., Patterson, C., Mittal, S., 2020. Predicting bioavailability of monoclonal antibodies after subcutaneous administration: open innovation challenge. Adv. Drug Deliv. Rev. 167, 66–77. https://doi.org/10.1016/j.addr.2020.05.009.
Sanhajariya, S., Duffull, S.B., Isbister, G.K., 2018. Pharmacokinetics of snake venom. Toxins 10. https://doi.org/10.3390/toxins10020073.
Sanhajariya, S., Isbister, G.K., Duffull, S.B., 2020. The influence of the different disposition characteristics of snake toxins on the pharmacokinetics of snake venom. Toxins 12, 188. https://doi.org/10.3390/toxins12030188.
Schneider, E.L., Hearn, B.R., Pfaff, S.J., Fontaine, S.D., Reid, R., Ashley, G.W., Grabulovski, S., Strassberger, V., Vogt, L., Jung, T., Santi, D.V., 2016. Approach for half-life extension of small antibody fragments that does not affect tissue uptake. Bioconjugate Chem. 27, 2534–2539. https://doi.org/10.1021/acs.bioconjchem.6b00469.
Seifert, S.A., Boyer, L.V., 2001. Recurrence phenomena after immunoglobulin therapy for snake envenomations: part 1. Pharmacokinetics and pharmacodynamics of immunoglobulin antivenoms and related antibodies. Ann. Emerg. Med. 37, 189–195. https://doi.org/10.1067/mem.2001.113135.
Serrano, S.M.T., 2013. The long road of research on snake venom serine proteinases. Toxicon, Milest. Future Prospects Snake Venom Res. 62, 19–26. https://doi.org/10.1016/j.toxicon.2012.09.003.
Sevcik, C., D'Suze, G., Díaz, P., Salazar, V., Hidalgo, C., Azpúrua, H., Bracho, N., 2004. Modelling Tityus scorpion venom and antivenom pharmacokinetics. Evidence of active immunoglobulin G's F(ab')2 extrusion mechanism from blood to tissues. Toxicon 44, 731–741. https://doi.org/10.1016/j.toxicon.2004.07.032.
Shah, D.K., Betts, A.M., 2013. Antibody biodistribution coefficients. mAbs 5, 297–305. https://doi.org/10.4161/mabs.23684.
Sim, S.M., Saremi, K., Tan, N.H., Fung, S.Y., 2013. Pharmacokinetics of Cryptelytrops purpureomaculatus (mangrove pit viper) venom following intravenous and intramuscular injections in rabbits. Int. Immunopharm. 17, 997–1001. https://doi.org/10.1016/j.intimp.2013.10.007.
Six, D.A., Dennis, E.A., 2000. The expanding superfamily of phospholipase A2 enzymes: classification and characterization. Biochim. Biophys. Acta Mol. Cell Biol. Lipids 1488, 1–19. https://doi.org/10.1016/S1388-1981(00)00105-0.
Skerra, A., 2007. Alternative non-antibody scaffolds for molecular recognition. Curr. Opin. Biotechnol. Protein Technol./Syst. Biol. 18, 295–304. https://doi.org/10.1016/j.copbio.2007.04.010.
Stillman, N.R., Kovacevic, M., Balaz, I., Hauert, S., 2020. In silico modelling of cancer nanomedicine, across scales and transport barriers. npj Computat. Mater. 6, 1–10. https://doi.org/10.1038/s41524-020-00366-8.
Tan, C.H., Liew, J.L., Tan, K.Y., Tan, N.H., 2016a. Assessing SABU (Serum Anti Bisa Ular), the sole Indonesian antivenom: a proteomic analysis and neutralization efficacy study. Sci. Rep. 6, 37299 https://doi.org/10.1038/srep37299.
Tan, K.Y., Tan, C.H., Fung, S.Y., Tan, N.H., 2016b. Neutralization of the principal toxins from the venoms of Thai Naja kaouthia and Malaysian hydrophis schistosus: insights into toxin-specific neutralization by two different antivenoms. Toxins 8, 86. https://doi.org/10.3390/toxins8040086.
Tasoulis, T., Isbister, G.K., 2017. A review and database of snake venom proteomes. Toxins 9. https://doi.org/10.3390/toxins9090290.
van Faassen, H., Ryan, S., Henry, K.A., Raphael, S., Yang, Q., Rossotti, M.A., Brunette, E., Jiang, S., Haqqani, A.S., Sulea, T., MacKenzie, C.R., Tanha, J., Hussack, G., 2020. Serum albumin-binding VHHs with variable pH sensitivities enable tailored half-life extension of biologics. Faseb. J. 34, 8155–8171. https://doi.org/10.1096/fj.201903231R.
Vázquez, H., Olvera, F., Alagón, A., Sevcik, C., 2013. Production of anti-horse antibodies induced by IgG, F(ab')2 and Fab applied repeatedly to rabbits. Effect on antivenom pharmacokinetics. Toxicon 76, 362–369. https://doi.org/10.1016/j.toxicon.2013.09.004.
Vázquez, H., Olvera, F., Paniagua-Solís, J., Alagón, A., Sevcik, C., 2010. Pharmacokinetics in rabbits and anti-sphingomyelinase D neutralizing power of Fab, F(ab')2, IgG and IgG(T) fragments from hyper immune equine plasma. Int. Immunopharm. 10, 447–454. https://doi.org/10.1016/j.intimp.2010.01.005.
Wang, J., Iyer, S., Fielder, P.J., Davis, J.D., Deng, R., 2016. Projecting human pharmacokinetics of monoclonal antibodies from nonclinical data: comparative evaluation of prediction approaches in early drug development. Biopharm Drug Dispos. 37, 51–65. https://doi.org/10.1002/bdd.1952.
Wilson, B.Z., Bahadir, A., Andrews, M., Karpen, J., Winkler, G., Smelski, G., Dudley, S., Walter, F.G., Shirazi, F.M., 2022. Initial Experience with F(ab')2 Antivenom Compared with Fab Antivenom for Rattlesnake Envenomations Reported to a Single Poison Center during 2019. Toxicon. https://doi.org/10.1016/j.toxicon.2022.01.007.
Wu, F., Bhansali, S.G., Law, W.C., Bergey, E.J., Prasad, P.N., Morris, M.E., 2012. Fluorescence imaging of the lymph node uptake of proteins in mice after subcutaneous injection: molecular weight dependence. Pharm. Res. (N. Y.) 29, 1843–1853. https://doi.org/10.1007/s11095-012-0708-6.
Yap, M.K.K., Fung, S.Y., Tan, K.Y., Tan, N.H., 2014a. Proteomic characterization of venom of the medically important Southeast Asian Naja sumatrana (Equatorial spitting cobra). Acta Trop. 133, 15–25. https://doi.org/10.1016/j.actatropica.2014.01.014.
Yap, M.K.K., Tan, N.H., Sim, S.M., Fung, S.Y., 2013. Toxicokinetics of Naja sputatrix (Javan spitting cobra) venom following intramuscular and intravenous administrations of the venom into rabbits. Toxicon 68, 18–23. https://doi.org/10.1016/j.toxicon.2013.02.017.
Yap, M.K.K., Tan, N.H., Sim, S.M., Fung, S.Y., Tan, C.H., 2014b. Pharmacokinetics of Naja sumatrana (equatorial spitting cobra) venom and its major toxins in experimentally envenomed rabbits. PLoS Neglected Trop. Dis. 8 https://doi.org/10.1371/journal.pntd.0002890.
Yates, J.W.T., Arundel, P.A., 2008. On the volume of distribution at steady state and its relationship with two-compartmental models. J. Pharmaceut. Sci. 97, 111–122. https://doi.org/10.1002/jps.21089.